Elsevier Editorial System(tm) for Geochimica et Cosmochimica Acta

Manuscript Draft

Manuscript Number: GCA-D-19-00956R2

Title: Melt chemistry and redox conditions control titanium isotope fractionation during magmatic differentiation

Article Type: Article

Corresponding Author: Mr. Liam Hoare, M.S

Corresponding Author's Institution: Cardiff University

First Author: Liam Hoare, M.S

Order of Authors: Liam Hoare, M.S; Martijn Klaver, PhD; Nikitha Saji, PhD; Jamie Gillies, M.S; Ian J Parkinson, PhD; C. Johan Lissenberg, PhD; Marc-Alban Millet, PhD

Abstract: Titanium offers a burgeoning isotope system that has shown significant promise as a tracer of magmatic processes. Recent studies have shown that Ti displays significant mass-dependent variations linked to the crystallisation of Fe-Ti oxides during magma differentiation. We present a comprehensive set of Ti isotope data for a range of differentiation suites from alkaline (Ascension Island, Afar and Heard Island), calc-alkaline (Santorini) and tholeiitic (Monowai seamount and Alarcon Rise) magma series to further explore the mechanics of Ti isotope fractionation in magmas. Whilst all suites display an increase in δ49/47Ti (deviation in 49Ti/47Ti of a sample relative to the OL-Ti reference material) during magma differentiation relative to indices such as increasing SiO2 and decreasing Mg#, our data reveal that each of the three magma series have contrasting δ49/47Ti fractionation patterns over comparable ranges of SiO2 and Mg#. Alkaline differentiation suites from intraplate settings display the most substantial range of variation (δ49/47Ti = +0.01 to +2.32‰), followed by tholeiites (-0.01 to +1.06‰) and calc-alkaline magmas (+0.06 to +0.64‰). Alkaline magmas possess high initial melt TiO2 contents which enables early saturation of ilmenite + titanomagnetite and a substantial degree of oxide crystallisation, whereas tholeiitic and calc-alkaline suites crystallise less oxide and have titanomagnetite as the dominant oxide phase. Positive slopes of FeO*/TiO2 vs. SiO2 during magma differentiation are related to high degrees of crystallisation of Ti-rich oxides (i.e. ilmenite). Bulk solid-melt Ti isotope fractionation factors co-vary with the magnitude of the slope of FeO*/TiO2 vs. SiO2 during magma differentiation, this indicates that the modal abundance and composition of the Fe-Ti oxide phase assemblage, itself is controlled by melt composition, governs Ti isotope fractionation during magma evolution. In addition to this overall control, hydrous, oxidised calc-alkaline suites display a resolvable increase in δ49/47Ti at higher Mg# relative to drier and more reduced tholeiitic arc suites. These subparallel Ti isotope fractionation patterns are best explained by the earlier onset of oxide segregation in arc magmas with a higher oxidation state and H2O content. This indicates the potential of Ti isotopes to be utilised as proxies for geodynamic settings of magma generation.

Melt chemistry and redox conditions control titanium isotope fractionation during magmatic differentiation

Liam Hoare[a]*, Martijn Klaver[a], Nikitha S. Saji[a**], Jamie Gillies[a], Ian J. Parkinson[b], C. Johan Lissenberg[a] and Marc-Alban Millet[a]

[a]School of Earth and Ocean Sciences, Cardiff University, Park Place, Cardiff, CF10 3AT, UK
[b]School of Earth Science, University of Bristol, Wills Memorial Building, Queens Road, Bristol, BS8 1RJ, UK

*Corresponding author: hoarel2@cardiff.ac.uk
**now at: Centre for Star and Planet Formation, University of Copenhagen, Øster Voldgade 5-7 DK-1350, Copenhagen, Denmark

Abstract

Titanium offers a burgeoning isotope system that has shown significant promise as a tracer of magmatic processes. Recent studies have shown that Ti displays significant mass-dependent variations linked to the crystallisation of Fe-Ti oxides during magma differentiation. We present a comprehensive set of Ti isotope data for a range of differentiation suites from alkaline (Ascension Island, Afar and Heard Island), calc-alkaline (Santorini) and tholeiitic (Monowai seamount and Alarcon Rise) magma series to further explore the mechanics of Ti isotope fractionation in magmas. Whilst all suites display an increase in $\delta^{49/47}$Ti (deviation in ^{49}Ti/^{47}Ti of a sample relative to the OL-Ti reference material) during magma differentiation relative to indices such as increasing SiO_2 and decreasing Mg#, our data reveal that each of the three magma series have contrasting $\delta^{49/47}$Ti fractionation patterns over comparable ranges of SiO_2 and Mg#. Alkaline differentiation suites from intraplate settings display the most substantial range of variation ($\delta^{49/47}$Ti = +0.01 to +2.32‰), followed by tholeiites (-0.01 to +1.06‰) and calc-alkaline magmas (+0.06 to +0.64‰). Alkaline magmas possess high initial melt TiO_2 contents which enables early saturation of ilmenite + titanomagnetite and a substantial degree of oxide crystallisation, whereas tholeiitic and calc-alkaline suites crystallise less oxide and have titanomagnetite as the dominant oxide phase. Positive slopes of FeO^*/TiO_2 vs. SiO_2 during magma differentiation are related to high degrees of crystallisation of Ti-rich oxides (i.e. ilmenite). Bulk solid-melt Ti isotope fractionation factors co-vary with the magnitude of the slope of FeO^*/TiO_2 vs. SiO_2 during magma differentiation, this indicates that the modal abundance and composition of the Fe-Ti oxide phase assemblage, itself is controlled by melt composition, governs Ti isotope fractionation during magma evolution. In addition to this overall control, hydrous, oxidised calc-alkaline suites display a resolvable increase in $\delta^{49/47}$Ti at higher Mg# relative to drier and more reduced tholeiitic arc suites. These subparallel Ti isotope fractionation patterns are best explained by the earlier onset of oxide segregation in arc magmas with a higher oxidation state and H_2O content. This indicates the potential of Ti isotopes to be utilised as proxies for geodynamic settings of magma generation.

Keywords: Titanium isotopes; magmatic differentiation; isotope fractionation; titanomagnetite; ilmenite; water content

1. Introduction

As a result of recent advances in mass spectrometry a growing arsenal of non-traditional mass-dependent isotope systems have been applied to investigate the evolution of the Earth and other terrestrial bodies in the solar system, such as Mg (Teng et al., 2010; Hin et al., 2017), Ca (Simon and DePaolo, 2010; Chen et al., 2019), Fe (Craddock and Dauphas, 2011; Debret et al., 2016), Cr (Bonnand et al., 2016; Schoenberg et al., 2016), V (Prytulak et al., 2013; Prytulak et al., 2016; Sossi et al., 2018) and Ni (Klaver et al., 2020). In particular, analytical advances have enabled increasing application of non-traditional isotopes to study high temperature processes, such as magmatic differentiation, where magnitudes of equilibrium isotope fractionation were generally inferred to be too small to resolve prior to the advent of high resolution MC-ICP-MS (Zhang et al., 2011; Millet et al., 2012; Millet and Dauphas, 2014; Teng et al., 2015; Willbold et al., 2016; McCoy-West et al., 2017; Nanne et al., 2017). Titanium is a refractory lithophile element that is highly fluid-immobile and abundant in igneous rocks. It has been used extensively within igneous geochemistry to trace magmatic processes and mantle source composition, including delineating island arc signatures in the geologic record (e.g. Pearce and Cann, 1973; Shervais, 1982) and more recently, enriched mantle sources in ocean islands (Prytulak and Elliott, 2007).In stark contrast to the use of Ti concentrations,, the mass-dependent isotopic composition of Ti has only recently been investigated and applied as a novel isotopic tool to study magmatic processes (Millet et al., 2016; Greber et al., 2017; Deng et al., 2018; Deng et al., 2019; Johnson et al., 2019).

Titanium is present in several co-ordination states within magmatic systems: it predominantly exists in 5-fold co-ordination in silicate melts but can also occupy 4-fold and 6-fold co-ordination in silicic and mafic melts respectively (Farges et al., 1996; Farges and Brown, 1997). Mass-dependent isotope fractionation theory dictates that equilibrium mass-dependent isotope fractionation is driven by contrasts in co-ordination number, which by extension control bond strength, with heavy isotopes preferring stronger bonds and vice versa (e.g. Schauble, 2004; Young et al., 2015). As the Ti budget of igneous rocks is controlled by Fe-Ti oxides, such as titanomagnetite ($Fe^{2+}[Fe^{3+},Ti]_2O_4$) and ilmenite ($FeTiO_3$), in which Ti is predominantly hosted in 6-fold sites, the crystallisation of Fe-Ti oxides should consequentially be the main driver of Ti isotope fractionation in magmatic systems, with $\delta^{49/47}$Ti progressively increasing from basaltic to rhyolitic compositions (Millet et al., 2016, Deng et al., 2019, Johnson et al., 2019). Because Fe-Ti oxide saturation in magmatic systems is controlled in part by the intimate link between magma redox state and water content, this suggests that Ti isotopes have the potential to provide insights into the oxidation state and water content of mantle melts. This property hold promise because, in contrast to other redox sensitive elements such as Fe (Sossi et al., 2012;

Dauphas et al., 2014) and V (Prytulak et al., 2016; Sossi et al., 2018), Ti only exists in one valence state in terrestrial magmatic environments as Ti^{4+} (Millet et al., 2016). This removes the additional complexity of mass-dependent isotope fractionation between different redox states e.g. Fe^{2+} and Fe^{3+} (Williams et al., 2004; Sossi et al., 2012; Dauphas et al., 2014).

Previous work (Millet et al., 2016; Deng et al., 2019; Johnson et al., 2019, Wang et al., 2020) has demonstrated the utility of Ti isotopes as tracers of oxide-melt equilibrium. These studies report magmatic samples exhibiting a progressive increase in $\delta^{49/47}Ti_{OL\text{-}Ti}$ (deviation in $^{49}Ti/^{47}Ti$ in a sample relative to the OL-Ti reference material; hereafter written as $\delta^{49/47}Ti$) with increasing SiO_2 (wt%). This was attributed to the crystallisation of Fe-Ti oxides, in which isotopically light Ti is preferentially incorporated, thus enriching the remaining melt in heavy Ti isotopes. Greber et al. (2017) recently utilised this relationship in order to constrain the composition of continental crust through time, identifying Ti isotope signatures in Archean shales that indicate that they were likely derived from a felsic protolith. However, Deng et al. (2019) observed a greater range of fractionation in differentiated samples from sub-alkaline intraplate lavas from the Afar rift and Hekla in Iceland ($\delta^{49/47}Ti$ of -0.005 to +2.012‰) compared to that of the calc-alkaline Agung suite ($\delta^{49/47}Ti$ of +0.054 to +0.259‰) measured by Millet et al. (2016) and argued for an auxiliary role of melt structure linked to the propensity of more silicic melts to contain a higher proportion of Ti in 4-fold co-ordination (e.g. Farges et al., 1996, Farges and Brown, 1997). The current data set of mass-dependent Ti isotope data for differentiated samples is limited; hence, it is difficult to ascertain if other controls beside Fe-Ti oxide crystallisation exist. The main objective of this contribution is to present high-precision $\delta^{49/47}Ti$ measurements of complete differentiation suites in order to: (i) better quantify the fractionation behaviour of Ti isotopes during magmatic differentiation in different magmatic series (alkaline, calc-alkaline and tholeiitic); (ii) determine the presence of auxiliary controls to oxide-melt equilibrium that can either serve to help or hinder Ti isotope fractionation, such as discerning the significance of ilmenite versus titanomagnetite crystallisation as these phases have different Ti bonding environments and thus potentially different fractionation factors e.g. (Leitzke et al., 2018, Wang et al., 2020); and (iii) investigate the potential of Ti isotopes to serve as proxy for the conditions of magma evolution such as redox and melt H_2O content.

2. Sample context and background

In order to investigate the behaviour of Ti isotopes during magmatic differentiation, we selected a diverse range of predominantly basalt to rhyolite differentiation suites from different geodynamic settings with distinct differentiation trends; alkaline, calc-alkaline and tholeiitic. Whole rock major element variation diagrams and discrimination diagrams for these suites reveal distinct evolution patterns for each of the three magma series investigated here (Fig.1; see Table S1). This is particularly evident in K_2O and total alkalis, Mg#, and TiO_2 (Fig. 1).

Alkaline intraplate and tholeiitic lavas typically have low H_2O contents and are relatively reduced (Moore, 1970; Canil, 1999; Campbell, 2001; Dixon and Clague, 2001; Lee et al., 2005). In contrast, calc-alkaline arc magmas are H_2O-rich and oxidised, and hence would display earlier onset of Fe-Ti oxide saturation during magma differentiation (Toplis and Carroll, 1995; Howarth and Prevec, 2013; MacLeod et al., 2013; Nandedkar et al., 2014). Importantly, upon oxide saturation, oxidised magmas crystallise Fe-Ti oxides with lower Ti content than more reduced magmas (e.g. Toplis and Carrol, 1995; Berndt et al. 2005; Feig et al. 2010). Calc-alkaline lavas are dominated by titanomagnetite, with ilmenite only appearing in the late stages of differentiation, whereas in reduced magmas ilmenite tends to saturate earlier (e.g. Berndt et al., 2005; Feig et al., 2010). Since the pioneering work of Harker and Daly in the early 20^{th} century e.g. (Harker, 1909; Daly, 1914) it has been established that tholeiitic magmas are characterised by enrichments in TiO_2 and FeO during early stages of magma differentiation, that is less pronounced in calc-alkaline magmas due to earlier crystallisation of clinopyroxene and Fe-Ti oxides. Alkaline differentiation suites from intraplate settings display the largest enrichments in TiO_2 compared with both tholeiitic and calc-alkaline suites due to their origin as small melt fractions derived from enriched sources (e.g. Prytulak and Elliott, 2007) (Fig. 1 a and b). The salience of this origin is that their elevated TiO_2 contents enables them to stabilise both titanomagnetite and ilmenite during the early stages of magmatic differentiation (Toplis and Carroll, 1995). Additionally, these intraplate magmas tend to have an intermediate oxygen fugacity between that of mid-ocean ridge tholeiites and calc-alkaline arcs (Kress and Carmichael, 1991).

The suites measured in this study were selected based on the criteria that they are the product of magma differentiation by fractional crystallisation with very limited modification by magma mixing or hybridisation. Evidence for the general absence of magma mixing in the studied suites comes from the scarcity of reverse zoning and disequilibrium textures e.g. Ascension Island (Chamberlain et al., 2016; Chamberlain et al., 2019) and Santorini (Klaver, 2016), lack of radiogenic isotope variation in Agung (Dempsey, 2013), Heard Island (Barling et al., 1990a,b, 1994a) and Monowai (Timm et al., 2011) or the preservation of the FeO*, TiO_2, and incompatible trace element enrichment along a single liquid line of descent in magmas recording the early stages of magma differentiation in Alarcon Rise (Clague et al., 2018), Monowai (Kemner et al., 2015) and the Afar Rift (Field et al., 2013). Whilst magma mixing is often invoked as the main mechanism of generation of intermediate arc magmas e.g. (Reubi and Blundy, 2009; Laumonier et al., 2014; Millet et al., 2014), Santorini is unusual as its eruptive products are the result of low-pressure fractional crystallisation without significant magma mixing as indicated by patterns of major and trace element variation (Nicholls, 1971; Huijsmans et al., 1988; Huijsmans and Barton, 1989; Barton et al., 1983; Michaud et al., 2000; Zellmer et al., 2000). Volcanic units on Santorini that do show geochemical evidence for

magma mixing, such as the Therasia dome complex and Cape Riva Tuff (Fabbro et al., 2013), are excluded from this study.

A summary of both the intensive variables for each differentiation suite and Fe-Ti oxide petrography and composition is provided in Table 1. A brief summary of the geologic context of each sample suite is provided below.

Suite	*Stage*	*T (˚C)*	*P (MPa)*	*H_2O (wt%)*	*fO_2*	*Ti-mag*	*TiO_2 (wt%)*	*Ilm*	*TiO_2 (wt%)*
Afar	1	1205 - 848	430 - 100	~0.4	QFM +0.5 - -3.6	✓	22.7	✓	50.4
	2	1085 - 800				✓	18.1	✓	51.0
Ascension Island	1	1174 - 932	330 - 250	~0.5	NNO +0.5 - -2.3	✓	22.2	✓	45.7
	2	1034 - 772				✓	20.9	✓	50.1
*Heard Island**	1	1216 - 1076	≤ 350	~0.6	~ QFM	✓	19.3	✓	47.3
	2	1070 - 916				✓	15.0	✓	41.9
Santorini	1	1070 - 1000	400 - 200	~3-5	QFM +0.5 - NNO +1.5	minor	7.9	×	-
	2	1000 - 900				✓	11.6	rare	47.5
*Alarcon Rise**	1	1210 - 1100	100 - 20	~0.2	~ QFM-1	×	-	×	-
	2	1090 - 895				✓	22.5	minor	49.9
Monowai	1	1200 - 1100	≤ 300	< 1.1	n.a.	×	-	×	-
	2	1100 - 1080				✓	10.8	×	-

Table 1. Summary of intensive variables of magmatic differentiation and oxide petrogprahy for Afar (Field et al., 2013); Ascension Island (Chamberlain et al., 2019), Heard Island (Barling, 1990); Santorini (Andujar et al., 2015,2016); Alarcon Rise (Clague et al., 2018) and Monowai (Kemner et al., 2015) differentiation suites measured for their Ti isotopic composition in this study. * indicates intensive variables and Fe-Ti oxide compositions that are derived from Rhyolite MELTS (Gualda et al., 2012). H_2O (wt%) is based on estimates for the parental magma of each differentiation suite. Ti-mag = titanomagnetite, Ilm = ilmenite. TiO_2 (wt%) contents for titanomagnetite and ilmenite are average compositions taken from representative datasets from the cited literature and GEOROC (http://georoc.mpch-mainz.gwdg.de/georoc/) in the case of Santorini.

2.1. Alkaline differentiation suites

2.1.1. Dabbahu, Afar Rift, Ethiopia

The Afar samples were collected from Dabbahu composite volcano in the Manda-Hararo segment of the Afar Rift, Ethiopia in East Africa which has been active for over 67 ka (Field et al., 2013) and cover a compositional range from alkali basalt through trachyandesite to peralkaline rhyolite produced via closed system fractionation (Field et al., 2013). Samples in this study encompass a SiO_2 range of 47 to 75 and 8.5 wt% to 0.02 wt% in MgO, while TiO_2 contents of the Afar lavas range from 0.16 to 2.9 wt%, with the peak in TiO_2 occurring at a Mg# of 34. It is important to note that the Afar samples measured by Deng et al. (2019) are taken from the study of Pik et al. (2006), which were sampled from a

different part of the East African rift (Stratoid Series) than those measured in this study, and differ slightly in their bulk geochemistry. The Dabbahu sample set has a higher peak TiO_2 content, larger range of Mg# (Fig. 1, Table S1) and is moderately richer in alkalis (Fig. 1, Table S1). Both titanomagnetite and ilmenite are present as crystallising phases during the entirety of magma differentiation in Afar samples (Table 1), with the tendency for the modal proportion of ilmenite to increase in more evolved lavas (Field et al., 2013).

2.1.2. Ascension Island

Ascension Island is located in the southern Atlantic Ocean, 90 km west of the Mid-Atlantic Ridge. The onset of volcanism occurred 5-6 Ma ago, with subaerial volcanism occurring from ~ 1 Ma to present (Jicha et al., 2013; Preece et al., 2018). The samples are products of alkaline magmatism and fractional crystallisation (see Chamberlain et al., 2016; Chamberlain et al., 2019) and cover a similar compositional range to that of the Afar samples. SiO_2 contents range from 48 to 72.3 wt%, MgO contents from 6.1 to 0.1 wt%, and the TiO_2 contents from 0.23 to 2.9 wt% and the maximum in TiO_2 contents occurs at Mg# of 46.5. Similar to the Afar Rift, both mafic and felsic lavas have titanomagnetite and ilmenite in their crystal cargo, with the relative proportion of ilmenite versus titanomagnetite tending to increase in more intermediate and evolved lavas based on major and trace element modelling (Chamberlain et al., 2019).

2.1.3. Heard Island

The Heard Island samples were collected from the Laurens Peninsula Series on the Mt. Dixon volcanic cone (≤1 Ma; Clarke et al., 1983) from Heard Island in the southern Indian Ocean (Barling et al., 1990a,b, 1994a,b). The lavas of the Laurens Peninsula Series display a unique chemistry compared to other ocean island suites with extreme enrichments in TiO_2, encompassing a range of 0.7 to 5.4 wt% (Barling, 1994a) with the peak occurring at Mg# ~ 55. The lavas are also highly enriched in alkalis, being shoshonitic, and cover a compositional range of basanite to trachyandesite. The samples span a range in SiO_2 from 45. to 60 wt% and MgO contents range from 7.4 to 0.6 wt%. A striking petrologic feature of the Heard Island lavas in the unusually high modal abundance of Fe-Ti oxides (~17.5 - 20% of phenocrysts; titanomagnetite + ilmenite) in basanitic lavas (Table 1) which is reflective of their high initial TiO_2 contents (Barling et al., 1994a, b). Silicic lavas are less phyric but titanomagnetite and ilmenite are still dominant phenocryst phases (~5-15%; Barling et al., 1990a).

2.2. Calc-alkaline differentiation suites

2.2.1. Santorini

Eight samples were measured from Santorini volcano in the South Aegean Volcanic Arc, Greece (Klaver et al., 2016a; Klaver et al., 2016b). The Santorini samples (all <500 ka) form a complete medium to high-K calc-alkaline fractionation trend from basalt to rhyodacite. Santorini is the most hydrous differentiation suite sampled in this work with estimates of the initial H_2O contents in primitive lavas ranging from 3-5 wt% (Andújar et al., 2015). SiO_2 contents of the samples ranges from 51 to 71.5 wt%, 6.9 to 0.70 wt% for MgO, and TiO_2 contents ranging from 0.43 to 1.22 wt%, reaching a peak at Mg# of 44. On the basis of patterns of major and trace element variation the studied Santorini samples were generated mainly as a result of low-pressure fractional crystallisation under hydrous conditions (Nicholls, 1971; Huijsmans et al., 1988; Huijsmans and Barton, 1989; Michaud et al., 2000; Zellmer et al., 2000; Andujar et al., 2015, 2016). Primitive lavas in Santorini contain minor amounts of titanomagnetite (e.g. Nicholls, 1971), with the appearance of more Ti-rich titanomagnetites in andesitic and dacitic lavas, accompanied by minor ilmenite (Table 1; Nicholls, 1971).

2.3. Tholeiitic differentiation suites

2.3.1. Monowai seamount

The Monowai seamount is situated in the Tonga-Kermadec arc (Timm et al., 2011). The lavas range from tholeiitic basalts through to andesite, with their geochemical variation being consistent with fractional crystallisation under relatively anhydrous conditions (<1.1 wt% H_2O) acting as the major process based on petrography and patterns of major and trace element variation (Timm et al., 2011; Kemner et al., 2015). The SiO_2 contents of these samples range from 51 to 61 wt%, 6.9 to 1.0 wt% for MgO, with TiO_2 contents encompassing a range of 0.57 to 1.17 wt%, reaching a peak in TiO_2 contents at Mg# of 44.20. Petrography indicates the onset of titanomagnetite crystallisation at ~ 4 wt % MgO (Kemner et al., 2015). Magnetite is present in basaltic and basaltic andesite lavas as a groundmass phase, but major element variation and least squares modelling suggest it is Ti-poor (Kemner et al., 2015).

2.3.2. Alarcon Rise

Situated adjacent to the south eastern tip of Baja California (Mexico), Alarcon Rise forms part of the northernmost segment of the East Pacific Rise. It is a unique MORB

differentiation suite spanning a compositional range from basalt through to andesite and rhyolite with up to 77 wt% SiO_2 (Clague et al., 2018). Alarcon rise contains the first known rhyolites to have originated from a mid ocean ridge setting, with their geochemistry being consistent with petrogenesis via fractional crystallisation (Clague et al., 2018). The SiO_2 contents of samples selected for this study range from 49 to 77 wt%, 8.9 to 0.1 wt% for MgO. The peak TiO_2 contents of the suite ranges from 0.17 to 3.0 wt% with the peak coinciding with an Mg# of ~40. Fe-Ti oxide saturation in Alarcon Rise occurs at approximately ~4.5 wt% MgO, with titanomagnetite appearing first in the crystallising assemblage with minor ilmenite occurring in the more evolved lavas (Clague et al., 2018).

3. Analytical Methods

Samples measured during this study were processed and measured using the double spike procedure of Millet and Dauphas (2014). Between 10 and 50 mg of rock powder or glass chips (for Alarcon Rise samples) were digested in a 1:1 mixture of concentrated HNO_3 and HF on a hotplate at 120°C for 48 hrs. Following complete evaporation samples were then taken up in concentrated HNO_3 and dried down 3 times. Samples were then taken up in concentrated HCl. Approximately 40 mg of H_3BO_3 was added to ensure that any fluorides (which can sequester Ti from solution) are re-dissolved and all Ti from the sample is in solution. Following digestion, an aliquot corresponding to 5 µg of Ti is taken and equilibrated with a ^{47}Ti-^{49}Ti double spike in a 48:52 ratio (Millet and Dauphas, 2014). Chemical purification of Ti is achieved according to the procedure designed by Zhang et al. (2011). Titanium isotope ratios were measured on a Nu instruments Plasma II multi-collector ICP-MS at the Cardiff Earth Laboratory for Trace Element and Isotope Chemistry (CELTIC) at Cardiff University. Samples were introduced through an Aridus II desolvating nebuliser. Isotope measurements were performed in medium resolution mode. All sample measurements were bracketed by measurements of the OL-Ti reference material (Millet and Dauphas, 2014) to account for the possibility of small polyatomic interferences on ^{47}Ti and ^{48}Ti induced by the mass spectrometer. Raw data were processed offline utilising in-house double spike deconvolution codes written in Mathematica®. Uncertainties are expressed as 95% confidence intervals (c.i. hereafter). Repeated digestion and measurements of reference materials JB-2 ($\delta^{49}/^{47}$Ti = -0.03 ± 0.01, n=2), BHVO-2 (-0.01 ± 0.03, n=3), BCR-2 (0.00 ± 0.01, n=3), and RGM-2 (+0.56 ± 0.05, n=5) are in agreement with that of previous studies (e.g. Millet et al., 2016; Greber et al., 2017).

Major and trace element contents of selected Monowai and Afar samples (see supplementary table S1) were determined at Cardiff University. Samples were crushed in a Mn steel jaw crusher, followed by an agate ball mill to produce a fine powder. Loss on ignition was determined gravimetrically. Powdered samples were prepared for measurement following the methods utilised in McDonald and Viljoen (2006). Major and trace element measurements were

performed via inductively coupled plasma optical emission spectrometry (ICP-OES) and inductively coupled plasma mass spectrometry (ICP-MS) respectively. A detailed outline of the analytical procedures can also be found in McDonald and Viljoen (2006).

4. Results

Mass-dependent Ti isotopic compositions for all reference materials and samples measured in this study are provided in Supplementary table 1 (S1) and illustrated in Figure 2. Data from Millet et al. (2016); Deng et al. (2019) and Johnson et al. (2019) are included for comparison. Samples of all three magma series define broadly similar trends of increasing $\delta^{49/47}$Ti values with increasing SiO_2 (Fig. 2a), consistent with previous studies (Millet et al., 2016; Deng et al., 2019; Johnson et al., 2019), and decreasing Mg# (Fig. 2b), TiO_2 (Fig. 2c) and V contents (Fig. 2d). As first reported by Millet et al. (2016), no significant variation is exhibited across primitive basaltic samples from MORB (tholeiitic), OIB (alkaline) or arc settings (calc-alkaline/tholeiitic), which fall within analytical uncertainty and define the BSE value. Fractionation pathways are offset between the different magma series across a given SiO_2 or Mg# range yet are internally consistent within each magma series (Fig. 2). The following section outlines the $\delta^{49/47}$Ti isotopic variation within each magma series.

4.1. Alkaline differentiation suites

Alkaline samples measured in this study define a range from +0.01 ± 0.03 ‰ to +2.32 ± 0.03 ‰ (Fig. 2). The Afar suite spans the greatest compositional range ($\delta^{49/47}$Ti = +0.03 to +2.32 ‰), in comparison to Ascension (+0.01 to +2.09 ‰) and Heard (+0.05 to +0.89). The range of $\delta^{49/47}$Ti compositions observed in alkaline intraplate lavas is comparable to that recently observed in intraplate lavas measured by Deng et al. (2019; Hekla and Afar) and Johnson et al. (2019; Kilaeua Iki). At a given SiO_2 content, alkaline suites display a greater increase in $\delta^{49/47}$Ti relative to calc-alkaline and tholeiitic magma series, particularly at more silicic compositions (>65 wt% SiO_2; Fig. 2). Figure 2 shows that all three alkaline suites exhibit consistent patterns of $\delta^{49/47}$Ti variation with regard to both increasing SiO_2 and decreasing Mg#.

4.2. Calc-alkaline differentiation suites

The $\delta^{49/47}$Ti values of all calc-alkaline differentiation suites included in this study vary between +0.05 ± 0.03 ‰ and +0.64 ± 0.02 ‰. The Santorini suite displays a greater range of variation (+0.06 ‰ to +0.64 ‰) compared to Agung (+0.05 ‰ to +0.26 ‰, Fig. 2) which essentially encapsulates the entire range of $\delta^{49/47}$Ti variation observed thus far in calc-alkaline arc suites. Calc-alkaline suites display the least fractionation at a given SiO_2 content (Fig. 2a),

yet conversely display a larger increase in $\delta^{49/47}$Ti values at a higher Mg# in comparison to the tholeiitic differentiation suites of Monowai (tholeiitic island arc) and Alarcon Rise (MOR; Fig. 2b). Interestingly, whilst Santorini lavas exhibit a mild TiO_2 enrichment trend at high Mg# (Fig. 1b), they also exhibit a resolvable increase in $\delta^{49/47}$Ti over this Mg# range (Fig. 2b).

4.3. Tholeiitic differentiation suites

The $\delta^{49/47}$Ti composition of samples from the Monowai tholeiitic island arc suite ranges from -0.01 to +0.27, the smallest magnitude of fractionation of any suite measured in this study, whereas the mid-ocean ridge tholeiites from Alarcon Rise range from -0.01 to +1.06 (Fig. 2). When plotted against SiO_2, the $\delta^{49/47}$Ti values of the tholeiitic suites occupy a region between the alkaline and calc-alkaline suites (Fig. 2a). However, at a given Mg#, tholeiitic suites display lighter $\delta^{49/47}$Ti values compared to both calc-alkaline and alkaline magma series (Fig. 2b).

5. Discussion

5.1. Titanium isotope fractionation during magmatic differentiation in different settings

The mass-dependent Ti isotopic composition of samples from alkaline, calc-alkaline and tholeiitic differentiation suites reveals increases in $\delta^{49/47}$Ti that are correlated with indices of magmatic differentiation such as increasing SiO_2 content and decreasing Mg# (Fig. 2a and 2b). These results are congruous with and complimentary to earlier work (Millet et al., 2016; Deng et al., 2019). The onset of resolvable Ti isotope fractionation coincides with a decrease in TiO_2 contents in all suites apart from Santorini (Fig. 2c), and in V (Fig. 2d). This reinforces the postulation that these trends are the manifestation of fractional crystallisation of Fe-Ti oxides, namely titanomagnetite and ilmenite (Millet et al., 2016; Johnson et al., 2019). Thus the main driver of Ti isotope fractionation is the proclivity for Fe-Ti oxides to extract light Ti isotopes from the melt, due to the co-ordination number contrast between Fe-Ti oxides (predominantly 6-fold) and melt (dominantly 5-fold with minor 6-fold; see Farges et al. (1996) and Farges and Brown (1997)).

A recent study by Deng et al. (2019), based on measurements of samples from the Afar rift (Pik et al., 2006) and Hekla (Savage et al., 2011), observed that sub-alkaline lavas from intraplate settings are more fractionated than differentiated lavas from other settings at a given SiO_2 content. Our data reveal that each of the three magma series, alkaline, calc-alkaline and tholeiitic display distinct $\delta^{49/47}$Ti fractionation patterns across multiple indices of magmatic differentiation (Fig. 2). Importantly, the majority of $\delta^{49/47}$Ti data in the literature have been reported with SiO_2 contents as the sole differentiation index. In this particular compositional space, alkaline suites display greater Ti isotope fractionation at a given SiO_2 content relative to

tholeiitic and calc-alkaline suites respectively (Fig. 2a). The offset in Ti isotopic compositions between the three magma series is particularly apparent at the more evolved end of the fractionation paths (>65 wt% SiO_2), with samples from alkaline suites surpassing the range recorded in the other suites by >1 ‰ (Fig. 2). It is noteworthy that the evolved lavas of intraplate settings are depleted in TiO_2 (0.2-0.4 wt% for samples with SiO_2 >65 wt%) relative to those of arc settings (0.3 – 1.0 wt% for samples with SiO_2 >65 wt%). This is consistent with i) large amounts of Fe-Ti oxide crystallisation (e.g. Barling et al., 1990b) and ii) evolved lavas from intraplate settings being the products of high degrees (>80%) of fractional crystallisation (e.g. Chamberlain et al., 2019), hence the fraction of Ti remaining in the melt is lower and in accordance with the lever rule the Ti isotopic variation between primitive and evolved melts is enhanced (Fig. 2c).

Contrasting patterns of fractionation emerge depending on the differentiation index used (i.e. SiO_2 content or Mg#), which can be utilised to better constrain the mechanisms of Ti isotope fractionation in magmas. In $\delta^{49/47}$Ti-Mg# space, calc-alkaline suites display higher $\delta^{49/47}$Ti values relative to tholeiitic suites at a given Mg# (Fig. 2b), with tholeiitic series exhibiting the smallest increase in $\delta^{49/47}$Ti at a given Mg# (Fig. 2b). These observations (compared to SiO_2) can be accounted for by the more oxidised and H_2O-rich nature of calc-alkaline magmas, which serves to supress the onset of plagioclase fractionation and enable the earlier crystallisation of clinopyroxene and Fe-Ti oxides during magma evolution (Gaetani et al., 1993; Sisson and Grove, 1993; Grove et al., 2003; Howarth and Prevec, 2013; Nandedkar et al., 2014). This effect promotes a faster increase in SiO_2 relative to a slower decrease in Mg# during differentiation of oxidised magmas, thus leading to different trajectories during magma evolution observed between Figures 2a and 2b.

Our data also show a systematic offset between alkaline and tholeiitic magma suites, with alkaline suites always displaying higher $\delta^{49/47}$Ti relative to tholeiitic suites at a given SiO_2 or Mg#. This might be related to the generally higher TiO_2 content of alkaline lavas, which controls the composition of the oxide phase(s) at equilibrium (Toplis and Carroll, 1995). The effect of melt chemistry on the composition of the oxide phase is best seen in Figure 3, in which the evolution of TiO_2 concentration and FeO^*/TiO_2, which are both strongly controlled by the composition of the oxide phase (e.g. Shellnut et al., 2009), is shown with respect to SiO_2. The evolution of FeO^*/TiO_2 with respect to SiO_2 can be divided into two distinct stages (stage 1 and stage 2) for each differentiation suite (Fig. 3). Each of the three magma series displays a sharp contrast in slope (i.e. $d(FeO^*/TiO_2)/dSiO_2$ and $dTiO_2/dSiO_2$) between the two stages (Fig 3). The slope $d(FeO^*/TiO_2)/dSiO_2$ ranges from negative in stage 1 of tholeiitic suites to positive in alkaline suites. The $d(FeO^*/TiO_2)/dSiO_2$ slopes of stage 2 are consistently more positive than their stage 1 counterparts in each differentiation suite (Fig. 3).

The range of $d(FeO^*/TiO_2)/dSiO_2$ displayed in our sample suites is best explained by the crystallisation of oxides of varying compositions, from Ti-poor (negative slopes) to Ti-rich

(positive slopes). This is corroborated by petrographic evidence indicating that slope inflections in Fig. 3 are the manifestation of changes in the crystallising oxide phase during magmatic differentiation. Indeed, samples that fall within stage 1 of alkaline suites contain high-Ti titanomagnetite (>19 wt% TiO_2) and a minor amount of ilmenite (>48 wt% TiO_2; Table 1), whereas both calc-alkaline and tholeiitic suites lack ilmenite in stage 1. Calc-alkaline suites (Santorini) crystallise minor amounts of titanomagnetite and display a weak negative slope. All tholeiitic suites lack Fe-Ti oxide phenocrysts during stage 1 and display strong negative slopes. The onset of stage 2 in alkaline suites corresponds to the increase in the modal proportion of ilmenite relative to Ti-magnetite (Table 1). In contrast for both calc-alkaline and tholeiitic suites, titanomagnetite becomes dominant and more Ti-rich than in stage 1. This results in $d(FeO^*/TiO_2)/dSiO_2$ that is more positive in stage 2 relative to stage 1 yet less positive than in alkaline suite due to the absence of significant amount of ilmenite.

5.2. Modelling Ti isotope fractionation during magmatic differentiation

As noted by Deng et al. (2019) the Ti concentration of silicic melts (>65 wt% SiO_2) from different magmatic series are roughly comparable, yet their $\delta^{49/47}$Ti compositions differ considerably (Fig. 2). This suggests that differences in the crystal phases segregated and/or the total amount of crystallisation during magma evolution in different magma series control the Ti elemental and isotopic budget of magmas. Here we investigate these contrasts using linear regressions (Fig. 4).

The fraction of Ti in a melt (expressed as –ln *f*Ti in order to linearise fractionation relationships, see below) is derived using the relative differences in concentrations of TiO_2 and the average of two highly incompatible trace elements (for which the bulk K_d is <<1 and can effectively be assumed to be 0) that show consistent enrichment patterns with increasing differentiation (Rb and Th, Rb and Ba, Rb and La, and Ba or La where appropriate, see Table S1) between any sample and the most primitive sample of each suite as a proxy for the fraction of remaining melt.

Bulk solid-melt fractionation factors ($\alpha_{solid\text{-}melt}$) were derived empirically by taking a weighted least squares linear regression between the fraction of Ti remaining in the melt and the isotopic composition for each differentiation suite. Rearranging the conventional isotopic Rayleigh distillation equation for fractional crystallisation gives:

$$\ln\left(f\mathrm{Ti}\frac{R_A}{R_0}\right) = \alpha \ln f\mathrm{Ti}$$

Where *f*Ti is the fraction of Ti remaining in the melt, R_A/R_0 is the $^{49}Ti/^{47}Ti$ of a sample (A) relative to the most primitive sample (0) and α is the bulk solid-melt fractionation factor. The value of α, and related uncertainites, for a set of samples can then be obtained by weighted

least squares linear regression, which one was done for both stages of each sample suite (Figure 4).

As there are currently no published trace element data for the Alarcon Rise samples, the fractional crystallisation of this suite was modelled using the Rhyolite MELTS software (Gualda et al., 2012; Fig. S1). Using D395-R11 as a staring composition (Table S1) crystallisation occurs under parameters similar to those specified by Clague et al. (2018), with 0.2 wt % H_2O, a pressure of 800 bar and oxidation state of QFM-1 (Fig. S1). Following the approach of Millet et al. (2016), the Ti isotope evolution of the melt is then calculated using a Rayleigh distillation law and an isotope fractionation factor between Fe-Ti oxides and melt ($\Delta^{49/47}Ti_{oxide\text{-}melt}$) weighted according the proportion of Ti sequestered by Fe-Ti oxides at each step of the model. The best fit for the Alarcon Rise data was achieved using an empirical value of $\Delta^{49/47}Ti_{oxide\text{-}melt} = -0.38‰ \times 10^6/T^2$ (with T in K).

Titanium isotopic fractionation models reveal that no single fractionation factor can account for: (i) the full Ti isotopic evolution of all magma series; and (ii) the range of variation within individual differentiation suites. In all suites where a large range of magma differentiation is captured (i.e. from mafic to silicic magmas), the bulk solid-melt fractionation factors for stage 1 and 2 are significantly distinct (Fig. 4). The point at which each linear regression intersects the stage 1/stage 2 boundary from Fig. 3 are consistently within error (Fig. 4). Because both stages of magma evolution occur at different temperatures (Table 1), we first examine the effect of temperature on the magnitude of Ti isotope fractionation in stage 1 and 2 within each suite (Fig. 4).

5.3. The effect of temperature on Ti isotope fractionation

It has been well established that isotope fractionation factors (expressed as lnα) are proportional to $1/T^2$ (where T is the absolute temperature in Kelvin; e.g., Urey, 1947; Bigeleisen and Mayer, 1947; Schauble, 2004). As such, differences in observed fractionation factors between sample suites could be linked to difference in the temperature of magmatic differentiation between geodynamic settings and/or in magma storage conditions. However, two lines of argument indicate that temperature does not play a major role in the observed Ti isotope fractionation observed in our sample suites.

First, the decrease in temperature from stage 1 to stage 2 for all magma suites could be consistent with the decrease in the bulk $\alpha_{solid\text{-}melt}$. We tested the effect of temperature on modelled bulk crystal-melt fractionation factors by recalculating minimum and maximum $\alpha_{solid\text{-}melt}$ values for stage 1 over the published temperature range of stage 2 for each suite (Fig. 4). Temperatures ranges were derived using multiple techniques such as Fe-Ti oxide thermometry and various silicate-liquid thermometers including olivine, plagioclase and clinopyroxene (see Table 1 and references therein). The temperature-dependent models reveal that across all

three magma series, temperature only has a minor influence on the fractionation patterns, as all models demonstrate that simply decreasing the temperature is not sufficient to alter the stage 1 $\alpha_{solid\text{-}melt}$ in order to reach the increased $\delta^{49/47}Ti$ values observed in stage 2 (Fig. 4).

Second, our $\alpha_{solid\text{-}melt}$ values for both stage 1 and 2 do not follow a simple linear relationship with $1/T^2$ (Fig. 5) but instead $\alpha_{solid\text{-}melt}$ across all three magma series displays a large variation at a given temperature (Fig. 5). Both calc-alkaline and tholeiitic suites consistently display significantly smaller fractionation factors with decreasing temperature (increasing $1/T^2$) compared to alkaline suites (Fig. 5) Consequently, temperature only has a secondary control on Ti isotope fractionation during magma evolution and other factors such as melt chemistry and/or structure govern Ti isotope fractionation during magma differentiation.

5.4. Linking contrasting magnitudes of titanium isotope fractionation to melt composition

Titanium-bearing oxides host Ti in 6-fold co-ordinated sites, whereas Ti is dominantly present in 5-fold coordination in silicate melts relative to 6-fold co-ordinated Ti, with 4-fold co-ordinated Ti found in minor amounts only in silicic melts (Farges et al., 1996). Therefore, the appearance of 4-fold co-ordinated Ti during magma differentiation may lead to distinct fractionation patterns and increased isotope fractionation factors in silicic melts relative to mafic melts. The lack of detailed melt structure data for Ti makes it difficult to estimate how melt composition affects the Ti coordination as well as over what range of silica content 4-fold co-ordinated titanium appears and whether it coincides with the boundary between stage 1 and 2 (Figures 3 and 4). Nevertheless, the coordination environment in silicate melts can be qualitatively evaluated using an estimate of melt polymerisation such as NBO/T (i.e. the ratio between non-bridging oxygen and tetrahedrally co-ordinated cations; Mills, 1993). Across all the sample suites investigate in this study, it is notable that i) the decrease in NBO/T is monotonic over the entire SiO_2 range and ii) all suites broadly align on the same overall trend, thus indicating no major differences in their respective coordination environment (Fig. 6). Therefore, while more detailed studies of Ti coordination in silicate melts are warranted, it appears unlikely that melt structure plays a dominant role in controlling mass-dependent Ti isotope variations in magmatic systems.

In contrast, our data suggest that Ti isotope fractionation in magmas is controlled by the abundance and composition of oxides in the segregating crystal fraction, which itself is controlled by melt chemistry, especially melt FeO and TiO_2 content (e.g. Toplis and Carroll, 1995). The boundary between stage 1 and stage 2 does not occur at the same proportion of Ti remaining in the melt ($-\ln fTi$) in all suites, yet it is broadly consistent between suites of the same magma series and corresponds to major inflections in FeO^*/TiO_2 vs. SiO_2. Importantly, the least fractionated suites also have the most Ti remaining in the melt after stage 1 (c. 50% for tholeiitic series), followed by calc-alkaline (c. 25%) and alkaline (c. 15%). This reflects the

amount of Ti partitioning into the oxide phase, which increases from tholeiites to calc-alkaline and alkaline magmas.

The melt chemistry control on Ti isotope fractionation in magma is further indicated by a robust covariation between calculated solid-melt fractionation factors and $d(FeO^*/TiO_2)/dSiO_2$ (Fig. 7). This correlation holds for all stages and all suites (including those measured by Deng et al., 2019 and Johnson et al., 2019) apart from stage 1 of tholeiitic suites, in which there is no resolvable fractionation (Fig. 4). All fractionation factors are recalculated to a common temperature of 1000˚C (Fig. 7). The relationship in Fig. 7 can be described using a least squares regression as follows:

$$For \frac{d\left(\frac{FeO^*}{TiO_2}\right)}{dSiO_2} < -0.75 \ \propto_{solid-melt} = 1$$

$$For -0.75 < \frac{d\left(\frac{FeO^*}{TiO_2}\right)}{dSiO_2} \leq +1.6 :$$

$$\propto_{solid-melt} = -3.1E^{-4} \ (\pm 5E^{-5}) \times \frac{d\left(\frac{FeO^*}{TiO_2}\right)}{dSiO_2} + 0.9998 \ (\pm 3E^{-5})$$

This correlation suggests that the Ti content of Fe-Ti oxides plays an important role in controlling Ti isotope fractionation during magmatic differentiation, with Ti-rich oxides having a stronger affinity for light isotopes of Ti than Ti-poor oxides, which is consistent with the results of a recent ab-initio study of inter-mineral Ti isotope fractionation by Wang et al. (2020), with rutile (TiO_2) possessing a greater fractionation factor than that of ilmenite and geikielite ($MgTiO_3$). Wang et al. (2020) did not perform ab-initio calculations for titanomagnetite but postulated that variations in its Ti contents would also likely affect its fractionation factor. This observation is also consistent with studies of other isotope systems, namely Fe isotopes, in which spinel solid-solution plays an important role in controlling equilibrium Fe isotope fractionation factors (e.g. Roskosz et al., 2015). Studies of the crystal structure of Ti-bearing oxides indicate that while the Ti-O bonds in titanomagnetite (0.205-0.206 nm) are longer than in ilmenite (0.197-0.199 nm; Wechsler et al., 1984; Wechsler and Prewitt, 1984), they also display different crystal structure. Titanomagnetite has an inverse spinel structure with a Fd3m space group (e.g. Bragg 1915; Nishikawa 1915; Barth and Posnjak, 1932) which contains one IV-co-ordinated cation and two VI-co-ordinated cations per four oxygens. At high temperature (>850˚C), Fe and Ti can become randomly distributed between these sites, implying that some Ti in titanomagnetite may be hosted in 4-folded coordination (Wu and Mason, 1981; O'Neill and Navrotsky, 1983; Wechsler et al. 1984). No such disorder could be observed in the R3 space group of ilmenite up to a temperature of 1050˚C (Wechsler and Prewitt, 1984), where all $Ti^{4+}$is hosted in 6-fold coordination. Thus, the crystal structure of titanomagnetite provides a potential mechanism by which it does not fractionate Ti isotopes as much as ilmenite. In addition, such a

mechanism would also imply that the Ti isotope fractionation factor between titanomagnetite and melt should be linked to its Ti content for a given temperature.

5.5. Implications of redox conditions and water content on titanium isotope fractionation

Our data establishes that at, a given Mg#, calc-alkaline arc suites have a heavier Ti isotopic composition than tholeiitic suites (Fig. 2). However, when the three individual arc suites are examined in isolation, they define distinct Ti isotopic fractionation paths (Fig. 8). Primitive Santorini samples display an early increase in $\delta^{49/47}$Ti at high Mg#, compared to Agung, which in turn, is heavier than Monowai (Fig. 8). The resolvable Ti isotopic fractionation in basalts and basaltic andesites is a result of the early onset of Fe-Ti oxide crystallisation (Fig.8).

Basaltic magmas at Santorini have an estimated initial H_2O content of 3-5 wt% and fO_2 ~ QFM +0.5 (Andújar et al., 2015, 2016). Based on the methodology of Parman et al. (2010), which utilises Al_2O_3 vs. MgO fractionation paths as a proxy for the suppression of plagioclase to infer pre-eruptive H_2O contents, Dempsey (2013) derived initial H_2O contents of 2-3 wt% for the Agung suite. Based on major element trends and thermobarometry of basaltic glasses, Kemner et al. (2015) concluded that Monowai parental basalts contain between ~0.5-1.1 wt% H_2O and follow a typical tholeiitic and hence a reduced fractionation path.

The onset of Fe-Ti oxide crystallisation is dependent on the interplay between initial melt H_2O contents and fO_2. Toplis and Carroll (1995, 1996) demonstrated that the saturation temperatures of Fe-Ti oxides are dependent on fO_2, with oxidising conditions in calc-alkaline suites being favourable to the early saturation of titanomagnetite. Increasing the H_2O content in a melt depresses the temperature of when both Fe-Mg silicates and plagioclase appears on the liquidus, whereas magnetite crystallisation is independent of H_2O contents (e.g. Sisson and Grove, 1993; Berndt et al., 2005; Feig et al., 2010).

Experimental studies have examined the differentiation pathways of tholeiitic basalts (e.g. Berndt et al., 2005; Feig et al., 2010) and arc basalts (e.g. Sisson and Grove, 1993; Tatsumi and Suzuki, 2009; Andujar et al., 2015; Melekhova et al., 2015) under differing initial H_2O contents and fO_2 conditions. Hydrous experiments on arc basalt starting compositions produced both a higher modal abundance of Fe-Ti oxides and greater depletions in TiO_2 with increasing H_2O (e.g. Tatsumi and Suzuki, 2009; Andujar et al., 2015; Melekhova et al., 2015). Therefore, the pattern of Ti isotope fractionation observed in our arc differentiation suites is consistent with earlier oxide saturation, specifically titanomagnetite, in more hydrous and oxidised magmas (e.g. Gaetani et al., 1993; Sisson and Grove, 1993; Grove et al., 2003), such as Santorini and Agung. The latter have significantly higher initial H_2O contents than Monowai which sets differentiating magmas under different fO_2 conditions on distinct but subparallel trends in $\delta^{49/47}$Ti versus Mg# space (Fig. 8).

These results indicate that variation of Ti isotope fractionation between different arc differentiation suites is in part a function of contrasting magma water content and hence redox

conditions. Measurements of Ti isotopic variations in other arc differentiation suites that have well-constrained redox and H_2O information, will allow the calibration of Ti isotopes as a novel isotopic proxy for H_2O contents and fO_2 conditions in arc magmas.

6. Conclusion

This study presents a comprehensive investigation of the behaviour of mass-dependent Ti isotope variations in terrestrial magmatic systems in order to deduce the controls on its isotopic fractionation. The main conclusions of this study are as follows:

1. There are contrasting patterns of Ti isotope fractionation during magmatic differentiation between different magmatic environments related to the fractional crystallisation of isotopically light Fe-Ti oxides. Of the investigated magma series, alkaline differentiation suites from intraplate settings display the most substantial variation in their Ti isotopic composition ($\delta^{49/47}$Ti = +0.01 to +2.32‰), followed by tholeiites (-0.01 to +1.06‰) and calc-alkaline suites (+0.06 to +0.64‰).
2. The co-evolution of FeO*/TiO_2 and $\delta^{49/47}$Ti in differentiating magmas indicates that magnitude of Ti isotopic fractionation is dominantly controlled by the composition and abundance of Fe-Ti oxides. This, in turn, is linked to the Fe-Ti contents of primitive magmas. Alkaline suites have a much higher FeO* and TiO_2 melt content which enables the early crystallisation of titanomagnetite and ilmenite, and a higher modal abundance of Fe-Ti oxides in general. In contrast, titanomagnetite serves as the dominant control of the Ti budget in the other suites.
3. Arc suites show different Ti isotope fractionation paths that scale with the redox state and H_2O content of parental magmas. Hydrous, oxidised calc-alkaline suites like Santorini and Agung display an enrichment in heavier Ti isotopes at a given Mg# relative to drier and more reduced arc tholeiitic suites such as Monowai.

Acknowledgements

We are indebted to the following scientists who kindly provided access to their sample collection: Katy Chamberlain and Jenni Barclay (Ascension Island), Jane Barling (Heard Island), David Clague (Alarcon Rise), Jon Blundy (Afar) and Christian Timm (Monowai). The authors gratefully acknowledge Morten Andersen and Max Jansen for discussions as well as Anabel Morte-Rodenas, Lindsey Owen and Matthew Dumont for support in the laboratory. Authors also thank Iain MacDonald for bulk-rock ICP-OES and ICP-MS measurements. This manuscript also benefitted from the insightful editorial handling of Julie Prytulak as well as in depth comments by Matthias Willbold, Paolo Sossi, Zhengbin Deng, and an anonymous reviewer. L. H acknowledges support from a NERC GW4+ Doctoral Training Partnership studentship (NE/L002434/1). MAM acknowledges support from a NERC standard grant (NE/R001332/1) and a Royal Society Research Grant.

References

Andújar, J., Scaillet, B., Pichavant, M. and Druitt, T.H. (2015) Differentiation conditions of a basaltic magma from Santorini, and its bearing on the production of andesite in arc settings. *Journal of Petrology,* 56, 765-794.
Andújar, J., Scaillet, B., Pichavant, M. and Druitt, T.H. (2016) Generation conditions of dacite and rhyodacite via the crystallization of an andesitic magma. Implications for the plumbing system at Santorini (Greece) and the origin of tholeiitic or calc-alkaline differentiation trends in arc magmas. *Journal of Petrology,* 57, 1887-1920.
Barling, J., 1990a. The petrogenesis of the Newer Lavas of Heard Island, southern Indian Ocean (Doctoral dissertation, Monash University).
Barling, J. and Goldstein, S.L., 1990b. Extreme isotopic variations in Heard Island lavas and the nature of mantle reservoirs. *Nature*, 348, 59-62.
Barling, J., 1994a. Origin and evolution of a high-Ti ocean island basalt suite: the Laurens Peninsula Series, Heard Island, Indian Ocean. *Mineralogical Magazine*, 58, 49-50.
Barling, J., Golstein, S.L. and Nicholls, I.A., 1994b. Geochemistry of Heard Island (southern Indian Ocean): characterization of an enriched mantle component and implications for enrichment of the sub-Indian Ocean mantle. *Journal of Petrology*, 35, 1017-1053.
Barton, M., Salters, V.J.M. and Huijsmans, J.P.P., 1983. Sr isotope and trace element evidence for the role of continental crust in calc-alkaline volcanism on Santorini and Milos, Aegean Sea, Greece. *Earth and Planetary Science Letters*, 63, 273-291.
Barth, T.F. and Posnjak, E., 1932. Spinel structures: with and without variate atom equipoints. *Zeitschrift Für Kristallographie-Crystalline Materials*, 82, 325-341.
Berndt, J., Koepke, J. and Holtz, F., 2005. An experimental investigation of the influence of water and oxygen fugacity on differentiation of MORB at 200 MPa. *Journal of Petrology*, 46, 135-167.
Bigeleisen, J. and Mayer, M.G., 1947. Calculation of equilibrium constants for isotopic exchange reactions. *The Journal of Chemical Physics*, 15, 261-267.
Bonnand, P., Parkinson, I.J. and Anand, M. (2016) Mass-dependent fractionation of stable chromium isotopes in mare basalts: Implications for the formation and the differentiation of the Moon. *Geochimica et Cosmochimica Acta,* 175, 208-221.
Bragg, W.H., 1915. The structure of magnetite and the spinels. Nature, 95, 561-561.
Campbell, I.H. (2001) Identification of ancient mantle plumes. *Special Papers-Geological Society of America*, 5-22.
Canil, D. (1999) Vanadium partitioning between orthopyroxene, spinel and silicate melt and the redox states of mantle source regions for primary magmas. *Geochimica et Cosmochimica Acta,* 63, 557-572.
Chamberlain, K.J., Barclay, J., Preece, K., Brown, R.J. and Davidson, J.P. (2016) Origin and evolution of silicic magmas at ocean islands: Perspectives from a zoned fall deposit on Ascension Island, South Atlantic. *Journal of Volcanology and Geothermal Research,* 327, 349-360.
Chamberlain, K., Barclay, J., Preece, K., Brown, R. and Davidson, J. (2019) Lower Crustal Heterogeneity and Fractional Crystallisation Control Evolution of Small Volume Magma Batches at Ocean Island Volcanoes (Ascension Island, South Atlantic). *Journal of Petrology*, 60, 1489-1522.
Chen, C., Dai, W., Wang, Z., Liu, Y., Li, M., Becker, H. and Foley, S.F., 2019. Calcium isotope fractionation during magmatic processes in the upper mantle. *Geochimica et Cosmochimica Acta*, 249, 121-137.
Clague, D.A., Caress, D.W., Dreyer, B.M., Lundsten, L., Paduan, J.B., Portner, R.A., Spelz-Madero, R., Bowles, J.A., Castillo, P.R. and Guardado-France, R. (2018) Geology of the Alarcon Rise, Southern Gulf of California. *Geochemistry, Geophysics, Geosystems,* 19, 807-837.
Clarke, I., McDougall, I. and Whitford, D.J., 1983. Volcanic evolution of heard and Mc-Donald Islands, Southern Indian Ocean. In *Antarctic earth science. International symposium*. 4, 631-635.
Craddock, P.R. and Dauphas, N. (2011) Iron isotopic compositions of geological reference materials and chondrites. *Geostandards and Geoanalytical Research,* 35, 101-123.
Daly, R.A. (1914) Igneous rocks and their origin. McGraw-Hill book company, Inc.
Dauphas, N., Roskosz, M., Alp, E., Neuville, D., Hu, M., Sio, C., Tissot, F., Zhao, J., Tissandier, L. and Médard, E. (2014) Magma redox and structural controls on iron isotope variations in Earth's mantle and crust. *Earth and Planetary Science Letters,* 398, 127-140.
Debret, B., Millet, M.-A., Pons, M.-L., Bouilhol, P., Inglis, E. and Williams, H. (2016) Isotopic evidence for iron mobility during subduction. *Geology,* 44, 215-218.

Dempsey, S., Robert (2013) Geochemistry of volcanic rocks from the Sunda Arc. Durham University, Durham University theses.
Deng, Z., Chaussidon, M., Savage, P., Robert, F., Pik, R. and Moynier, F. (2019) Titanium isotopes as a tracer for the plume or island arc affinity of felsic rocks. *Proceedings of the National Academy of Sciences,* 116, 1132-1135.
Deng, Z., Moynier, F., Sossi, P. and Chaussidon, M. (2018) Bridging the depleted MORB mantle and the continental crust using titanium isotopes. *Geochemical Perspectives Letters,* 9, 11-15.
Dixon, J.E. and Clague, D.A. (2001) Volatiles in basaltic glasses from Loihi Seamount, Hawaii: Evidence for a relatively dry plume component. *Journal of Petrology,* 42, 627-654.
Fabbro, G.N., Druitt, T.H. and Scaillet, S., 2013. Evolution of the crustal magma plumbing system during the build-up to the 22-ka caldera-forming eruption of Santorini (Greece). *Bulletin of Volcanology*, *75*, 767.
Farges, F. and Brown, G.E. (1997) Coordination chemistry of titanium (IV) in silicate glasses and melts: IV. XANES studies of synthetic and natural volcanic glasses and tektites at ambient temperature and pressure. *Geochimica et Cosmochimica Acta,* 61, 1863-1870.
Farges, F., Brown, G.E. and Rehr, J.J. (1996) Coordination chemistry of Ti (IV) in silicate glasses and melts: I. XAFS study of titanium coordination in oxide model compounds. *Geochimica et Cosmochimica Acta,* 60, 3023-3038.
Feig, S.T., Koepke, J. and Snow, J.E., 2010. Effect of oxygen fugacity and water on phase equilibria of a hydrous tholeiitic basalt. *Contributions to Mineralogy and Petrology*, 160, 551-568.
Field, L., Blundy, J., Calvert, A. and Yirgu, G. (2013) Magmatic history of Dabbahu, a composite volcano in the Afar Rift, Ethiopia. *Bulletin of the Geological Society of America*, 125, 128-147.
Gaetani, G.A., Grove, T.L. and Bryan, W.B. (1993) The influence of water on the petrogenesis of subductionrelated igneous rocks. *Nature,* 365, 332-334.
Greber, N.D., Dauphas, N., Puchtel, I.S., Hofmann, B.A. and Arndt, N.T. (2017) Titanium stable isotopic variations in chondrites, achondrites and lunar rocks. *Geochimica et Cosmochimica Acta,* 213, 534-552.
Grove, T.L., Elkins-Tanton, L.T., Parman, S.W., Chatterjee, N., Müntener, O. and Gaetani, G.A. (2003) Fractional crystallization and mantle-melting controls on calc-alkaline differentiation trends. *Contributions to Mineralogy and Petrology,* 145, 515-533.
Gualda, G.A., Ghiorso, M.S., Lemons, R.V. and Carley, T.L. (2012) Rhyolite-MELTS: a modified calibration of MELTS optimized for silica-rich, fluid-bearing magmatic systems. *Journal of Petrology,* 53, 875-890.
Harker, A. (1909) The natural history of igneous rocks. Macmillan, New York.
Helz, R.T., 1987. Differentiation behavior of Kilauea Iki lava lake, Kilauea Volcano, Hawaii: an overview of past and current work. *Magmatic processes: physicochemical principles*, 1, 241-258.
Helz, R.T. (2012) Trace-element analyses of core samples from the 1967-1988 drillings of Kilauea Iki lava lake, Hawaii, US Geological Survey Open File Report 2012–1050 (2012). US Department of the Interior, US Geological Survey, pp. US Geological Survey Open File Report 2012–1050.
Helz, R.T., Kirschenbaum, H., Marinenko, J. and Qian, R. (1994) Whole-rock analyses of core samples from the 1967, 1975, 1979 and 1981 drillings of Kilauea Iki lava lake, Hawaii, U.S. Geol. Survey Open File Report: 94-684. US Geological Survey, U.S. Geol. Survey.
Hin, R.C., Coath, C.D., Carter, P.J., Nimmo, F., Lai, Y.-J., von Strandmann, P.A.P., Willbold, M., Leinhardt, Z.M., Walter, M.J. and Elliott, T. (2017) Magnesium isotope evidence that accretional vapour loss shapes planetary compositions. *Nature,* 549, 511-515.
Höskuldsson, Á., Óskarsson, N., Pedersen, R., Grönvold, K., Vogfjörð, K. and Ólafsdóttir, R., 2007. The millennium eruption of Hekla in February 2000. *Bulletin of volcanology*, *70*, 169-182.
Howarth, G.H. and Prevec, S.A. (2013) Hydration vs. oxidation: modelling implications for Fe–Ti oxide crystallisation in mafic intrusions, with specific reference to the Panzhihua intrusion, SW China. *Geoscience Frontiers*, 4, 555-569.
Huijsmans, J.P. and Barton, M. (1989) Polybaric geochemical evolution of two shield volcanoes from Santorini, Aegean Sea, Greece: evidence for zoned magma chambers from cyclic compositional variations. *Journal of Petrology,* 30, 583-625.
Huijsmans, J.P., Barton, M. and Salters, V.J. (1988) Geochemistry and evolution of the calc-alkaline volcanic complex of Santorini, Aegean Sea, Greece. *Journal of Volcanology and Geothermal Research, 34*, 283-306.

Jicha, B.R., Singer, B.S. and Valentine, M.J., 2013. $^{40}Ar/^{39}Ar$ geochronology of subaerial Ascension Island and a re-evaluation of the temporal progression of basaltic to rhyolitic volcanism. *Journal of Petrology*, 54, 2581-2596.
Johnson, A.C., Aarons, S.M., Dauphas, N., Nie, N.X., Zeng, H., Helz, R.T., Romaniello, S.J. and Anbar, A.D. (2019) Titanium Isotopic Fractionation in Kilauea Iki Lava Lake Driven by Oxide Crystallization. *Geochimica et Cosmochimica Acta*, 264, 180-190.
Kemner, F., Haase, K.M., Beier, C., Krumm, S. and Brandl, P.A. (2015) Formation of andesite melts and Ca-rich plagioclase in the submarine Monowai volcanic system, Kermadec arc. *Geochemistry, Geophysics, Geosystems*, 16, 4130-4152.
Klaver, M. (2016) Dynamics of magma generation and differentiation in the central-eastern Aegean arc: A geochemical and petrological study of Quaternary arc volcanism in Greece, Department of Earth Sciences, Vrije Universiteit, Amsterdam Vrije Universiteit, Vrije Universiteit, Amsterdam
Klaver, M., Carey, S., Nomikou, P., Smet, I., Godelitsas, A. and Vroon, P. (2016a) A distinct source and differentiation history for Kolumbo submarine volcano, Santorini volcanic field, Aegean arc. *Geochemistry, Geophysics, Geosystems,* 17, 3254-3273.
Klaver, M., Davies, G.R. and Vroon, P.Z. (2016b) Subslab mantle of African provenance infiltrating the Aegean mantle wedge. *Geology*, 44, 367-370.
Klaver, M., Ionov, D.A., Takazawa, E. and Elliott, T., 2020. The non-chondritic Ni isotope composition of Earth's mantle. *Geochimica et Cosmochimica Acta*, 268, 405-421.
Kress, V.C. and Carmichael, I.S., 1991. The compressibility of silicate liquids containing Fe_2O_3 and the effect of composition, temperature, oxygen fugacity and pressure on their redox states. *Contributions to Mineralogy and Petrology*, 108, 82-92.
Laumonier, M., Scaillet, B., Pichavant, M., Champallier, R., Andujar, J. and Arbaret, L. (2014) On the conditions of magma mixing and its bearing on andesite production in the crust. *Nature Communications*, 5, 1-12.
Le Bas, M.J., Maitre, R.L., Streckeisen, A., Zanettin, B. and Rocks, I.S.o.t.S.o.I. (1986) A chemical classification of volcanic rocks based on the total alkali-silica diagram. *Journal of Petrology,* 27, 745-750.
Lee, C.-T., Leeman, W.P., Canil, D. and Li, Z.-X.A. (2005) Similar V/Sc systematics in MORB and arc basalts: implications for the oxygen fugacities of their mantle source regions. *Journal of Petrology,* 46, 2313-2336.
Leitzke, F.P., Fonseca, R.O.C., Göttlicher, J., Steininger, R., Jahn, S., Prescher, C. and Lagos, M., 2018. Ti K-edge XANES study on the coordination number and oxidation state of Titanium in pyroxene, olivine, armalcolite, ilmenite, and silicate glass during mare basalt petrogenesis. *Contributions to Mineralogy and Petrology*, 173, 103.
Lucic, G., Berg, A.S. and Stix, J., 2016. Water-rich and volatile-undersaturated magmas at Hekla volcano, Iceland. *Geochemistry, Geophysics, Geosystems*, *17*, 3111-3130.
MacLeod, C.J., Johan Lissenberg, C. and Bibby, L.E., 2013. "Moist MORB" axial magmatism in the Oman ophiolite: The evidence against a mid-ocean ridge origin. *Geology*, 41, 459-462.
McCoy-West, A.J., Millet, M.-A. and Burton, K.W. (2017) The neodymium stable isotope composition of the silicate Earth and chondrites. *Earth and Planetary Science Letters,* 480, 121-132.
McDonald, I. and Viljoen, K. (2006) Platinum-group element geochemistry of mantle eclogites: a reconnaissance study of xenoliths from the Orapa kimberlite, Botswana. *Applied Earth Science,* 115, 81-93.
Melekhova, E., Blundy, J., Robertson, R. and Humphreys, M.C., 2015. Experimental evidence for polybaric differentiation of primitive arc basalt beneath St. Vincent, Lesser Antilles. *Journal of Petrology*, 56, 161-192.
Michaud, V., Clocchiatti, R. and Sbrana, S. (2000) The Minoan and post-Minoan eruptions, Santorini (Greece), in the light of melt inclusions: chlorine and sulphur behaviour. *Journal of Volcanology and Geothermal Research, 99*, 195-214.
Millet, M.-A., Baker, J.A. and Payne, C.E. (2012) Ultra-precise stable Fe isotope measurements by high resolution multiple-collector inductively coupled plasma mass spectrometry with a ^{57}Fe-^{58}Fe spike*. Chemical Geology,* 304, 18-25.
Millet, M.-A. and Dauphas, N. (2014) Ultra-precise titanium stable isotope measurements by double-spike high resolution MC-ICP-MS. *Journal of Analytical Atomic Spectrometry,* 29, 1444-1458.

Millet, M.-A., Dauphas, N., Greber, N.D., Burton, K.W., Dale, C.W., Debret, B., Macpherson, C.G., Nowell, G.M. and Williams, H.M. (2016) Titanium stable isotope investigation of magmatic processes on the Earth and Moon. *Earth and Planetary Science Letters,* 449, 197-205.

Millet, M.A., Tutt, C.M., Handler, M.R. and Baker, J.A. (2014) Processes and time scales of dacite magma assembly and eruption at Tauhara volcano, Taupo Volcanic Zone, New Zealand. Geochemistry, *Geophysics, Geosystems,* 15, 213-237.

Mills, K.C., 1993. The influence of structure on the physico-chemical properties of slags. *ISIJ international*, 33,148-155.

Moore, J.G. (1970) Water content of basalt erupted on the ocean floor. *Contributions to Mineralogy and Petrology,* 28, 272-279.

Nandedkar, R.H., Ulmer, P. and Müntener, O. (2014) Fractional crystallization of primitive, hydrous arc magmas: an experimental study at 0.7 GPa. *Contributions to Mineralogy and Petrology, 167*, 1015.

Nanne, J.A., Millet, M.-A., Burton, K.W., Dale, C.W., Nowell, G.M. and Williams, H.M. (2017) High precision osmium stable isotope measurements by double spike MC-ICP-MS and N-TIMS. *Journal of Analytical Atomic Spectrometry,* 32, 749-765.

Nicholls, I. (1971) Petrology of Santorini Volcano, Cyclades, Greece. *Journal of Petrology,* 12, 67-119.

Nishikawa, S., 1915. Structure of some crystals of spinel group. *Proceedings of the Tokyo Mathematico-Physical Society*. 2nd Series, 8, 199-209.

O'Neill, H.S.C. and Navrotsky, A., 1983. Simple spinels; crystallographic parameters, cation radii, lattice energies, and cation distribution. *American Mineralogist*, 68(1-2), pp.181-194.

Parman, S., Grove, T., Kelley, K. and Plank, T. (2010) Along-arc variations in the pre-eruptive H_2O contents of Mariana arc magmas inferred from fractionation paths. *Journal of Petrology,* 52, 257-278.

Pearce, J.A. and Cann, J.R. (1973) Tectonic setting of basic volcanic rocks determined using trace element analyses. *Earth and Planetary Science Letters,* 19, 290-300.

Peccerillo, A. and Taylor, S. (1976) Geochemistry of Eocene calc-alkaline volcanic rocks from the Kastamonu area, northern Turkey. *Contributions to Mineralogy and Petrology,* 58, 63-81.

Pik, R., Marty, B. and Hilton, D. (2006) How many mantle plumes in Africa? The geochemical point of view. *Chemical Geology,* 226, 100-114.

Preece, K., Mark, D.F., Barclay, J., Cohen, B.E., Chamberlain, K.J., Jowitt, C., Vye-Brown, C., Brown, R.J. and Hamilton, S., 2018. Bridging the gap: $^{40}Ar/^{39}Ar$ dating of volcanic eruptions from the 'Age of Discovery'. *Geology*, 46, 1035-1038.

Roskosz, M., Sio, C.K., Dauphas, N., Bi, W., Tissot, F.L., Hu, M.Y., Zhao, J. and Alp, E.E., 2015. Spinel–olivine–pyroxene equilibrium iron isotopic fractionation and applications to natural peridotites. *Geochimica et Cosmochimica Acta*, *169*, pp.184-199.

Prytulak, J. and Elliott, T. (2007) TiO_2 enrichment in ocean island basalts. *Earth and Planetary Science Letters,* 263, 388-403.

Prytulak, J., Nielsen, S., Ionov, D., Halliday, A., Harvey, J., Kelley, K., Niu, Y., Peate, D.W., Shimizu, K. and Sims, K. (2013) The stable vanadium isotope composition of the mantle and mafic lavas. *Earth and Planetary Science Letters,* 365, 177-189.

Prytulak, J., Sossi, P., Halliday, A., Plank, T., Savage, P. and Woodhead, J. (2016) Stable vanadium isotopes as a redox proxy in magmatic systems. *Geochemical Perspectives Letters,* 3, 75-84.

Reubi, O. and Blundy, J. (2009) A dearth of intermediate melts at subduction zone volcanoes and the petrogenesis of arc andesites. *Nature,* 461, 1269-1273.

Rickwood, P.C. (1989) Boundary lines within petrologic diagrams which use oxides of major and minor elements. *Lithos,* 22, 247-263.

Savage, P.S., Georg, R.B., Williams, H.M., Burton, K.W. and Halliday, A.N. (2011) Silicon isotope fractionation during magmatic differentiation. *Geochimica et Cosmochimica Acta,* 75, 6124-6139.

Schauble, E.A. (2004) Applying stable isotope fractionation theory to new systems. *Reviews in Mineralogy and Geochemistry*, 55, 65-111.

Schoenberg, R., Merdian, A., Holmden, C., Kleinhanns, I.C., Haßler, K., Wille, M. and Reitter, E. (2016) The stable Cr isotopic compositions of chondrites and silicate planetary reservoirs. *Geochimica et Cosmochimica Acta,* 183, 14-30.

Shellnutt, J.G., Zhou, M.F. and Zellmer, G.F., 2009. The role of Fe–Ti oxide crystallization in the formation of A-type granitoids with implications for the Daly gap: an example from the Permian Baima igneous complex, SW China. *Chemical Geology*, *259*, 204-217.
Shervais, J.W. (1982) Ti-V plots and the petrogenesis of modern and ophiolitic lavas. *Earth and Planetary Science Letters,* 59, 101-118.
Simon, J.I. and DePaolo, D.J. (2010) Stable calcium isotopic composition of meteorites and rocky planets. *Earth and Planetary Science Letters,* 289, 457-466.
Sisson, T.W. and Grove, T.L., 1993. Experimental investigations of the role of H_2O in calc-alkaline differentiation and subduction zone magmatism. *Contributions to Mineralogy and Petrology*, 113, 143-166.
Sossi, P.A., Foden, J.D. and Halverson, G.P. (2012) Redox-controlled iron isotope fractionation during magmatic differentiation: an example from the Red Hill intrusion, S. Tasmania. *Contributions to Mineralogy and Petrology,* 164, 757-772.
Sossi, P.A., Prytulak, J. and O'Neill, H.S.C. (2018) Experimental calibration of vanadium partitioning and stable isotope fractionation between hydrous granitic melt and magnetite at 800 °C and 0.5 GPa. *Contributions to Mineralogy and Petrology,* 173, 27.
Tatsumi, Y. and Suzuki, T., 2009. Tholeiitic vs calc-alkalic differentiation and evolution of arc crust: constraints from melting experiments on a basalt from the Izu–Bonin–Mariana Arc. *Journal of Petrology*, 50, 1575-1603.
Teng, F.-Z., Li, W.-Y., Ke, S., Marty, B., Dauphas, N., Huang, S., Wu, F.-Y. and Pourmand, A. (2010) Magnesium isotopic composition of the Earth and chondrites. *Geochimica et Cosmochimica Acta,* 74, 4150-4166.
Teng, F.Z., Yin, Q.Z., Ullmann, C.V., Chakrabarti, R., Pogge von Strandmann, P.A., Yang, W., Li, W.Y., Ke, S., Sedaghatpour, F. and Wimpenny, J. (2015) Interlaboratory comparison of magnesium isotopic compositions of 12 felsic to ultramafic igneous rock standards analyzed by MC-ICPMS. *Geochemistry, Geophysics, Geosystems,* 16, 3197-3209.
Timm, C., Graham, I.J., de Ronde, C.E., Leybourne, M.I. and Woodhead, J. (2011) Geochemical evolution of Monowai volcanic center: New insights into the northern Kermadec arc subduction system, SW Pacific. *Geochemistry, Geophysics, Geosystems,* 12.
Toplis, M. and Carroll, M. (1995) An experimental study of the influence of oxygen fugacity on Fe-Ti oxide stability, phase relations, and mineral—melt equilibria in ferro-basaltic systems. *Journal of Petrology,* 36, 1137-1170.
Toplis, M. and Carroll, M. (1996) Differentiation of ferro-basaltic magmas under conditions open and closed to oxygen: implications for the Skaergaard intrusion and other natural systems. *Journal of Petrology*, 37, 837-858.
Urey, H.C., 1947. The thermodynamic properties of isotopic substances. *Journal of the Chemical Society (Resumed),* 562-581.
Wang, W., Huang, S., Huang, F., Zhao, X. and Wu, Z., 2020. Equilibrium inter-mineral titanium isotope fractionation: Implication for high-temperature titanium isotope geochemistry. *Geochimica et Cosmochimica Acta*, 269, 540-553.
Weber, G. and Castro, J.M., 2017. Phase petrology reveals shallow magma storage prior to large explosive silicic eruptions at Hekla volcano, Iceland. *Earth and Planetary Science Letters*, *466*, 168-180.
Wechsler, B.A., Lindsley, D.H. and Prewitt, C.T. (1984) Crystal structure and cation distribution in titanomagnetites (Fe_3-x$TixO_4$). *American Mineralogist,* 69, 754-770.
Wechsler, B.A. and Prewitt, C.T. (1984) Crystal structure of ilmenite ($FeTiO_3$) at high temperature and at high pressure. *American Mineralogist,* 69, 176-185.
Willbold, M., Hibbert, K., Lai, Y.J., Freymuth, H., Hin, R.C., Coath, C., Vils, F. and Elliott, T. (2016) High-precision mass-dependent molybdenum isotope variations in magmatic rocks determined by double-spike MC-ICP-MS. *Geostandards and Geoanalytical Research,* 40, 389-403.
Williams, H.M., McCammon, C.A., Peslier, A.H., Halliday, A.N., Teutsch, N., Levasseur, S. and Burg, J.-P. (2004) Iron isotope fractionation and the oxygen fugacity of the mantle. *Science,* 304, 1656-1659.
Wu, C.C. and Mason, T.O., 1981. Thermopower measurement of cation distribution in magnetite. *Journal of the American Ceramic Society*, 64, 520-522.

Young, E.D., Manning, C.E., Schauble, E.A., Shahar, A., Macris, C.A., Lazar, C. and Jordan, M. (2015) High-temperature equilibrium isotope fractionation of non-traditional stable isotopes: Experiments, theory, and applications. *Chemical Geology,* 395, 176-195.
Zellmer, G., Turner, S. and Hawkesworth, C. (2000) Timescales of destructive plate margin magmatism: new insights from Santorini, Aegean volcanic arc. *Earth and Planetary Science Letters,* 174, 265-281.
Zhang, J., Dauphas, N., Davis, A.M. and Pourmand, A. (2011) A new method for MC-ICPMS measurement of titanium isotopic composition: Identification of correlated isotope anomalies in meteorites. *Journal of Analytical Atomic Spectrometry,* 26, 2197-2205.

Figure Captions

Fig. 1. Whole rock major element variation and discrimination diagrams (a) TiO_2 vs SiO_2 ; (b) TiO_2 vs Mg#; (c) K_2O vs SiO_2 (Peccerillo and Taylor, 1976); (d) Total Alkalis vs. SiO_2 (Le Bas et al., 1986); for the differentiation suites measured in this study (see Table S1 and references therein) exhibiting the distinct major element fractional crystallisation paths characteristic of each suite; Alkaline (red), calc-alkaline (blue) and tholeiitic (green). Samples measured for Ti isotopic compositions are denoted by the larger empty symbols. Samples from Deng et al. (2019) are included for comparison. Boundary lines for K_2O vs SiO_2 and Total Alkalis vs. SiO_2 diagrams were taken from Rickwood (1989).

Fig. 2. Variations of $\delta^{49/47}$Ti (‰) versus (a) SiO_2 content, (b) Mg#, (c) TiO_2 and (d) V contents (where data is available). Uncertainties for $\delta^{49/47}$Ti (95% confidence interval measurement precision) are smaller than the size of the symbols.

Fig. 3. Whole rock TiO_2 vs. SiO_2 and FeO*/TiO_2 vs. SiO_2 diagrams of the differentiation suites measured in this study. Samples measured for Ti isotopic compositions are marked as gold crosses. Data are reported in Table S1. Inflections in both FeO*/TiO_2 vs. SiO_2 and TiO_2 vs. SiO_2 compositional space, indicated by the dashed lines, define two stages (stage 1 and stage 2) of evolution of each of the suites. These inflections mark either the appearance or change in the modal abundance and composition of Fe-Ti oxides (see section 5.2 for details).

Fig. 4. Ordinary least squares linear regressions of the Ti isotopic evolution of differentiation suites from each of the three magma series; (a) Afar (alkaline), (b) Ascension (alkaline), (c) Heard (alkaline), (d) Hekla (data from Deng et al., 2019; sub-alkaline), (e) Santorini (calc-alkaline) and (f) Monowai (tholeiitic). The fraction of Ti remaining in the melt (-ln*f*Ti) was calculated using incompatible trace elements (see Table S1). The Afar suite from Deng et al. (2019) could not be considered due to lack of available major and trace element data. Ordinary least regressions were performed for each of the two stages of melt evolution as defined by the major element relationships (Fig. 3), with the stage boundaries demarcated by the coloured dashed lines. Bulk $\alpha_{solid\text{-}melt}$ fractionation factors derived from weighted least squares regression (see section 5.2 for details). Bulk $\alpha_{solid\text{-}melt}$ values are labelled for each stage and are shown as dashed black lines. Shaded areas denote the 2s error envelope of the ordinary least squares linear regression. Stage 1 $\alpha_{solid\text{-}melt}$ values re-calculated at the recorded temperature ranges for stage 2 (see Table 1, temperature ranges for stage 1 and 2 of Hekla were sourced from Höskuldsson et al., 2007; Lucic et al., 2016; and Weber and Castro, 2017) are plotted as dashed black lines and show that the temperature decrease during magma differentiation cannot account for the observed range of Ti isotope fractionation (see section 5.3 for details).

Fig. 5. Bulk solid-melt fractionation factors ($\alpha_{solid\text{-}melt}$) plotted as a function of $1/T^2$ (K^{-2}). X axis error bars indicate the range of temperature taken from Table 1 for stage 1 and 2 (temperature ranges for stage 1 and 2 of Hekla were sourced from Höskuldsson et al., 2007; Lucic et al., 2016; and Weber and Castro, 2017). Dashed black lines indicate linear functions of $\alpha_{solid\text{-}melt}$ versus$1/T^2$ (K^{-2}).

Fig. 6. Variation of NBO/T (ratio of Non-Bridging Oxygen and Tetrahedrally co-ordinated cations; Mills, 1993) vs. SiO_2 for all differentiation suites (Alkaline, Calc-alkaline and Tholeiitic) measured for their Ti isotopic composition in this study.

Fig. 7. (a) Bulk solid-melt fractionation factors ($\alpha_{solid\text{-}melt}$) derived from weighted least squares regressions calculated at 1000˚C (Fig. 4) shown as a function of (dFeO*/TiO_2)/$d SiO_2$ values taken from Figure 3. Error bars display the 2s uncertainty on the data points. Error related to temperature ranges for each stage has been propagated. The black line indicates the least squares regression of the data, with the orange lines indicating the 2s uncertainty of the regression. Data from stage 1 of Tholeiitic suites are excluded from the regression as they display no resolvable fractionation. A co-variation trend (R^2=0.75) can be observed between decreasing $\alpha_{solid\text{-}melt}$ and increasing FeO*/TiO_2 slope. The (dFeO*/TiO_2)/$d SiO_2$ of Hekla is based on a representative dataset sourced from GEOROC (http://georoc.mpch-mainz.gwdg.de/georoc/), which includes all samples from Savage et al. (2011). For Kilauea Iki, (dFeO*/TiO_2)/$d SiO_2$ is based on selected whole rock and glass data from Helz et al. (1994) and Greaney et al. (2019) respectively; picrites and olivine basalts have undergone significant accumulation of olivine phenocrysts (Helz, 1987) and were therefore excluded. The value of -0.39 ± 0.06‰ ($\alpha_{solid\text{-}melt}$ = 0.99961) produced by Johnson et al. (2019) plotted for comparison and is in good agreement with the co-variation shown in Fig. 7. Figure symbols are identical to those shown in Figure 5.

Fig.8. Variations of $\delta^{49/47}$Ti versus Mg# for arc differentiation suites. Distinct fractionation patterns are observed for the different suites, with suites deriving from wetter and more oxidised parental magmas displaying earlier onset of Ti isotope fractionation linked to earlier onset of oxide saturation (see section 5.5 for details).

Figure 1

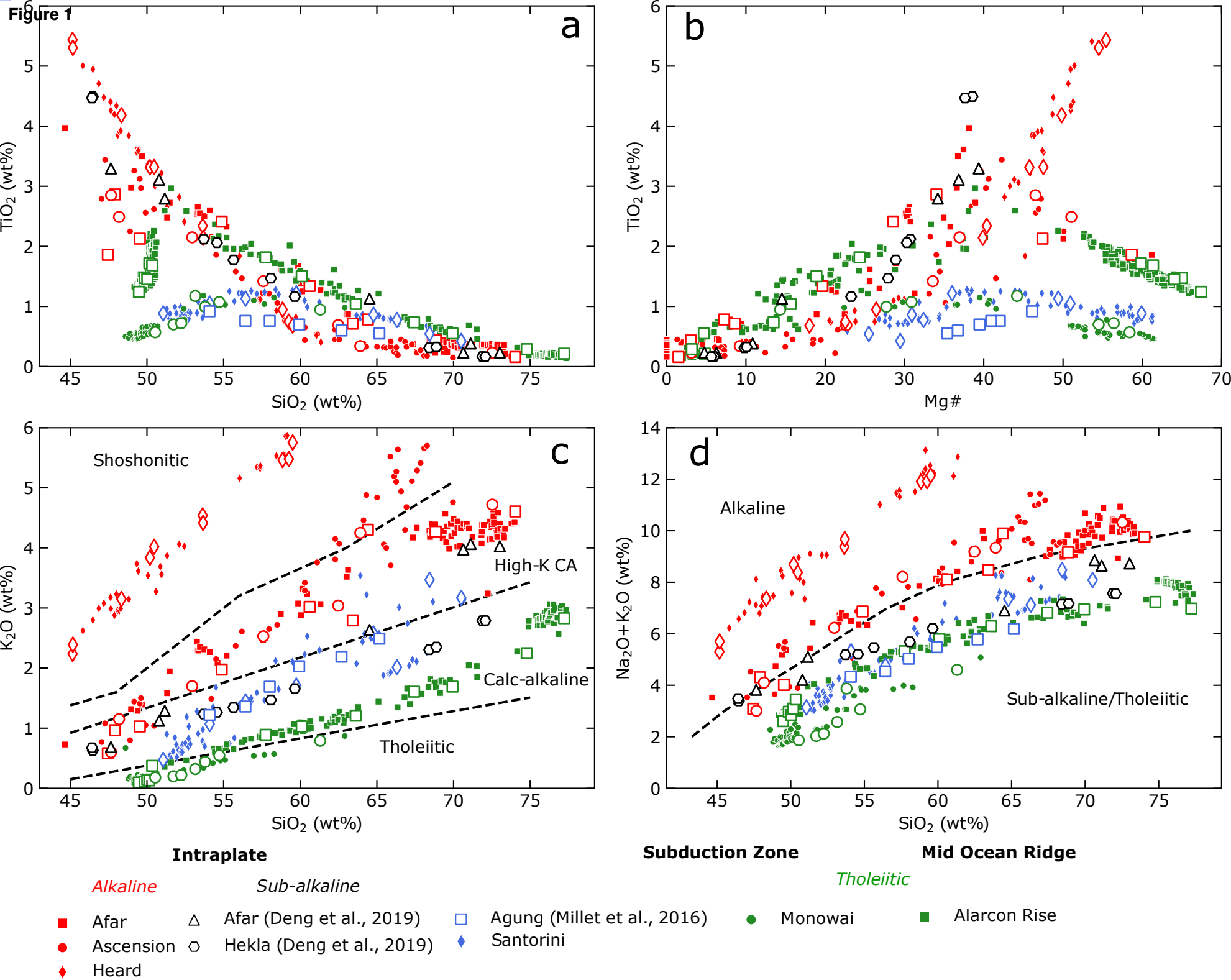
a
b
c
d
TiO2 (wt%)
SiO2 (wt%)
Mg#
K2O (wt%)
Na2O+K2O (wt%)
Shoshonitic
High-K CA
Calc-alkaline
Tholeiitic
Alkaline
Sub-alkaline/Tholeiitic
Intraplate
Subduction Zone
Mid Ocean Ridge
Alkaline
Sub-alkaline
Tholeiitic
Afar
Ascension
Heard
Afar (Deng et al., 2019)
Hekla (Deng et al., 2019)
Agung (Millet et al., 2016)
Santorini
Monowai
Alarcon Rise

Figure 2

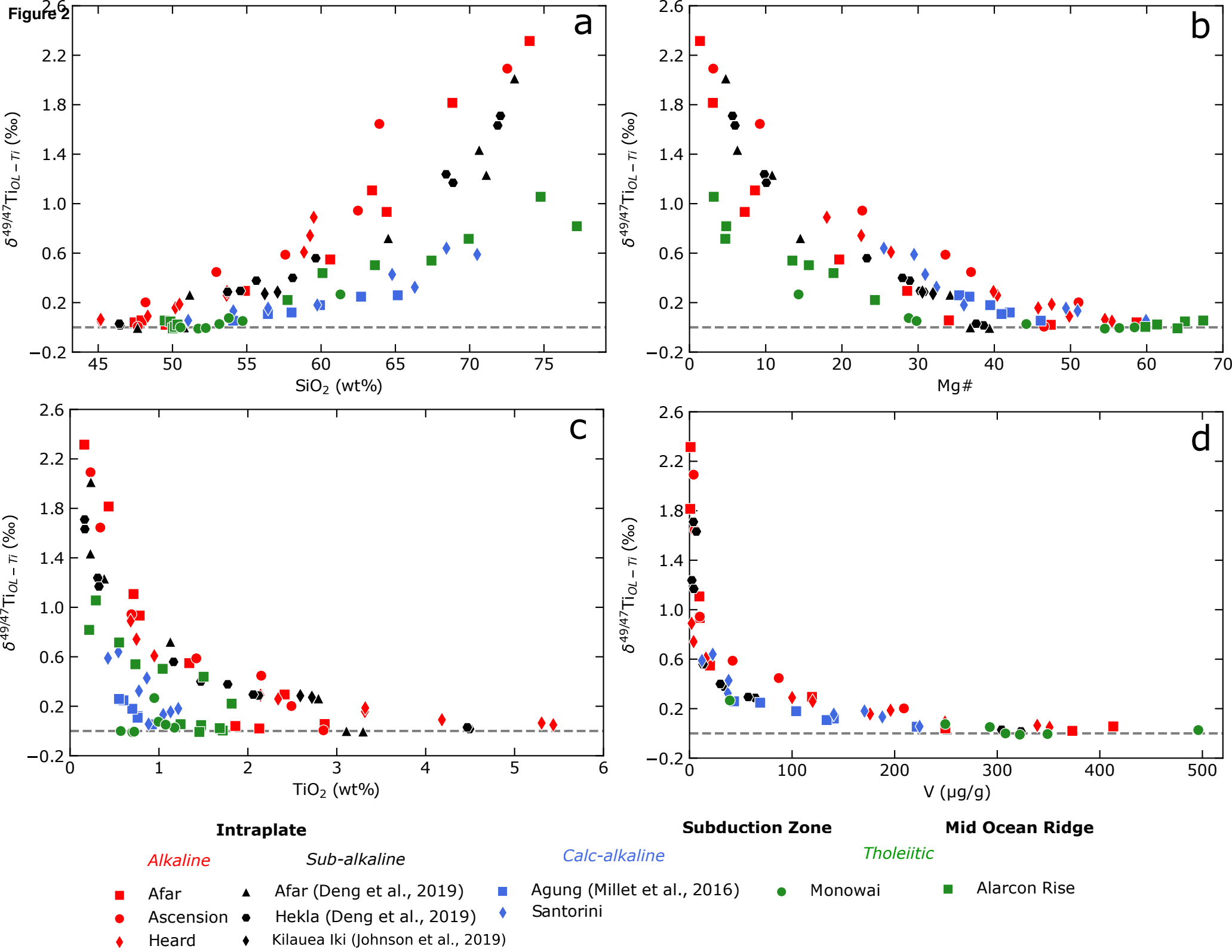
a
b
c
d
$\delta^{49/47}Ti_{OL-Ti}$ (‰)
SiO_2 (wt%)
Mg#
TiO_2 (wt%)
V (µg/g)
Intraplate
Subduction Zone
Mid Ocean Ridge
Alkaline
Sub-alkaline
Calc-alkaline
Tholeiitic
Afar
Ascension
Heard
Afar (Deng et al., 2019)
Hekla (Deng et al., 2019)
Kilauea Iki (Johnson et al., 2019)
Agung (Millet et al., 2016)
Santorini
Monowai
Alarcon Rise

Figure 3

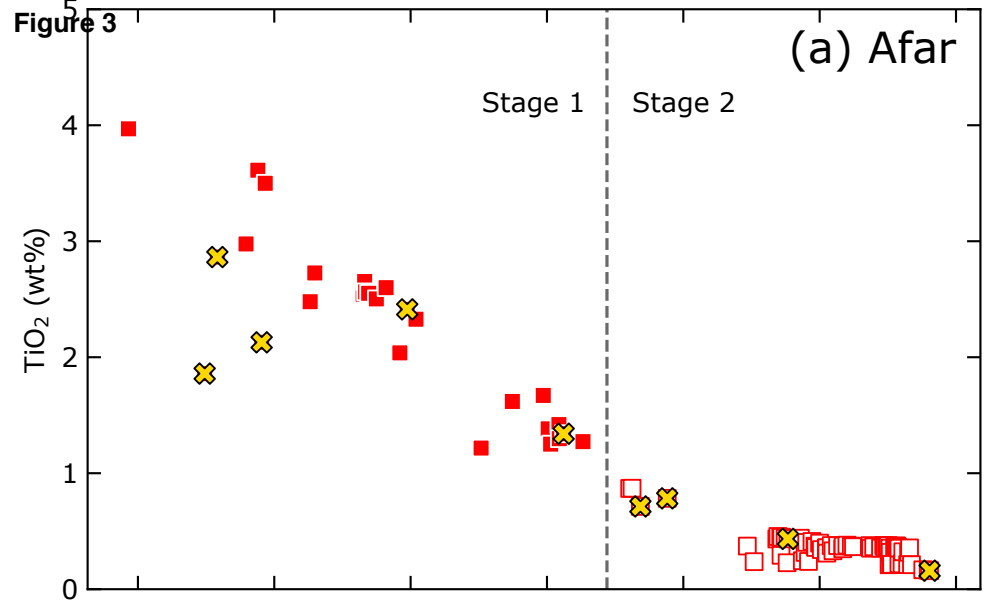
(a) Afar
Stage 1
Stage 2
TiO2 (wt%)

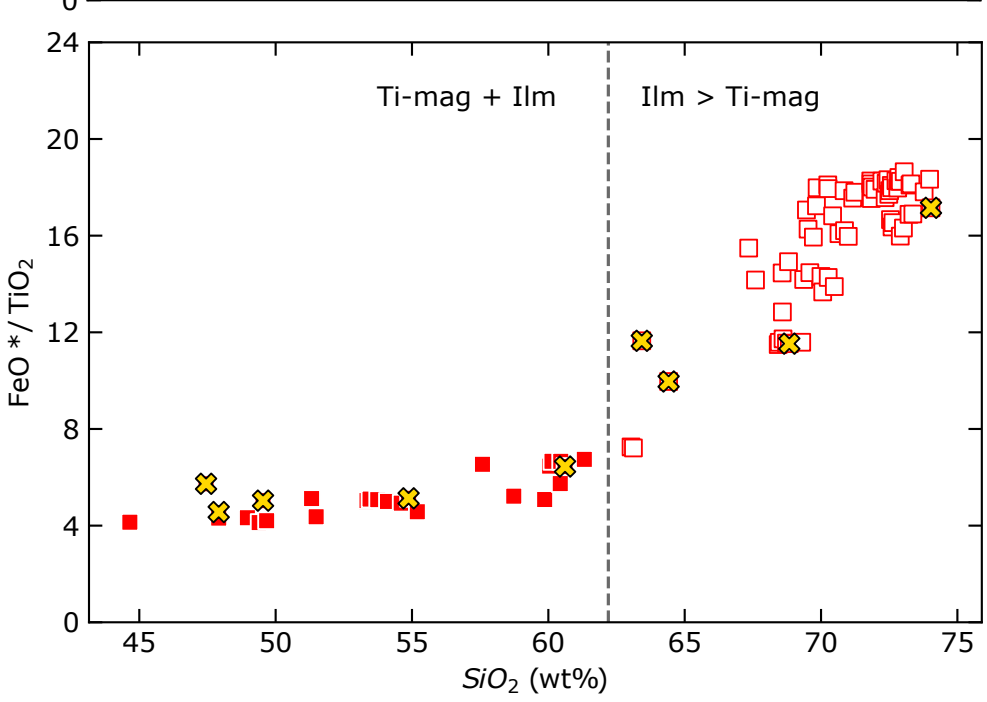
Ti-mag + Ilm
Ilm > Ti-mag
FeO * / TiO2
SiO2 (wt%)

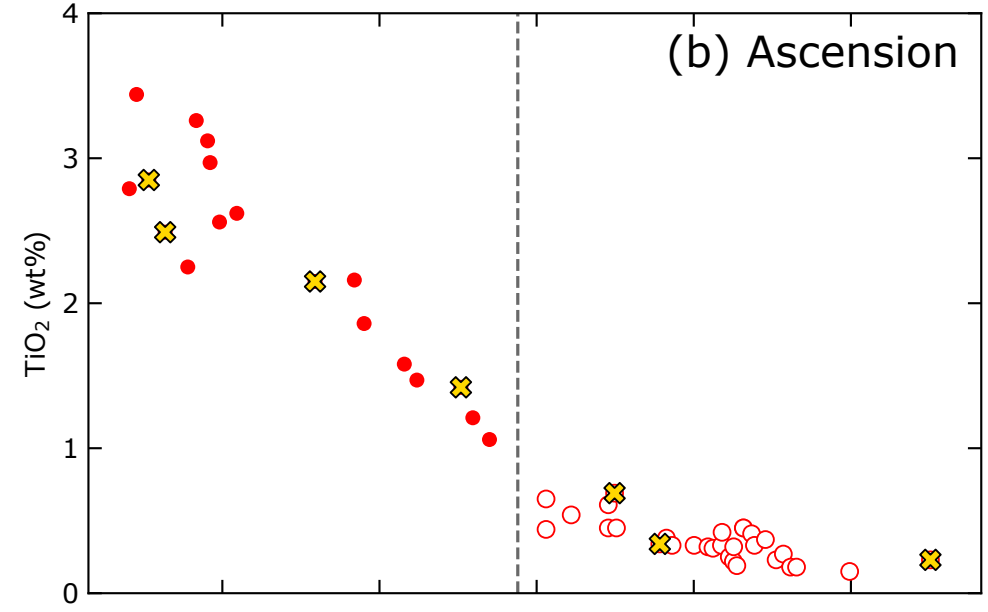
(b) Ascension
TiO2 (wt%)

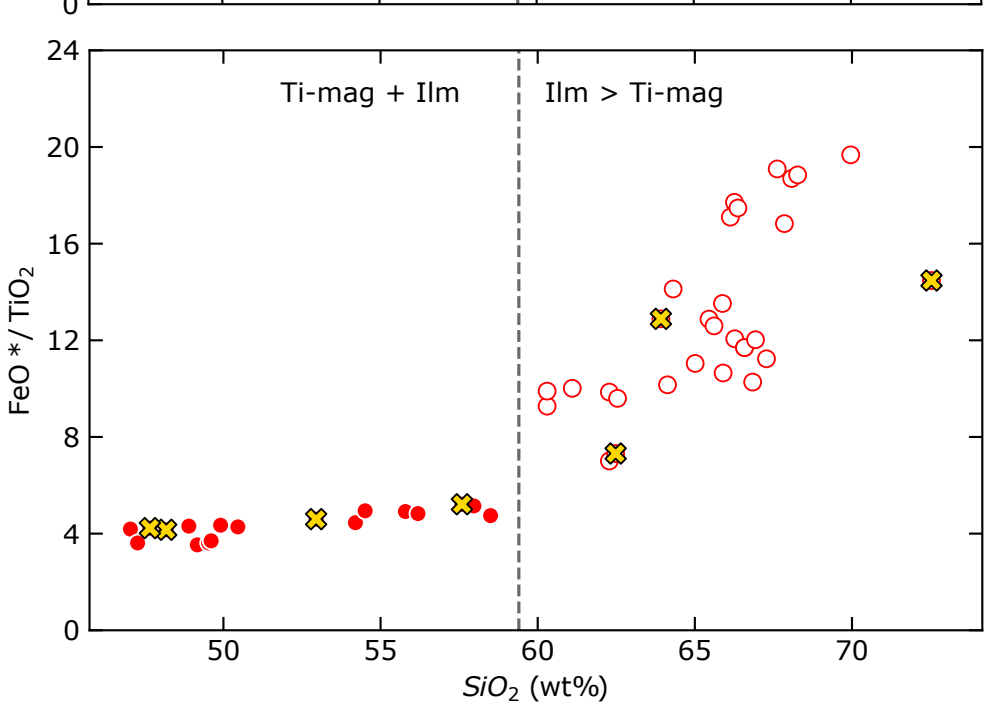
Ti-mag + Ilm
Ilm > Ti-mag
FeO * / TiO2
SiO2 (wt%)

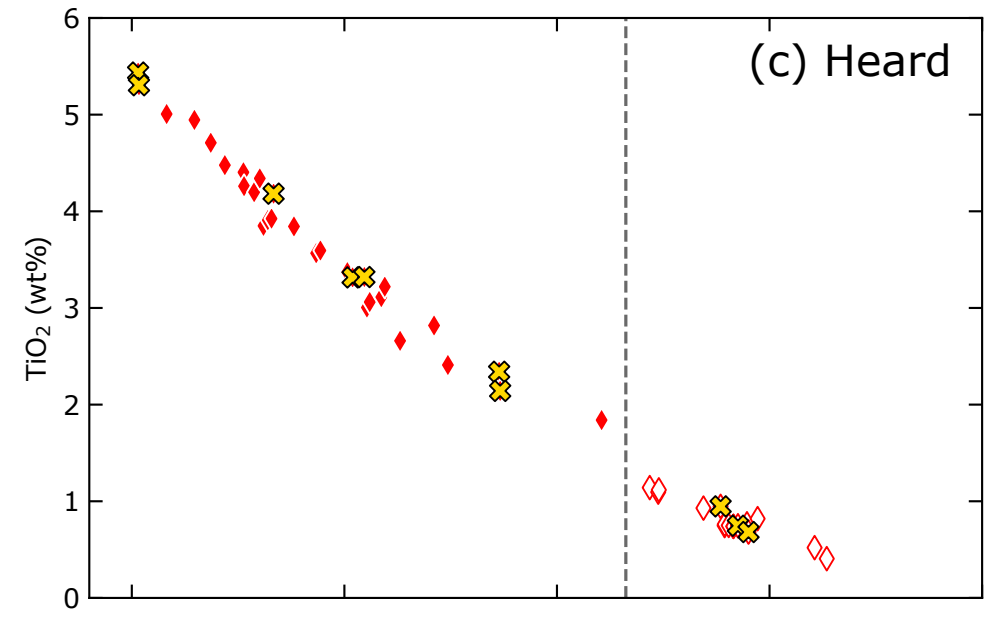
(c) Heard
TiO2 (wt%)

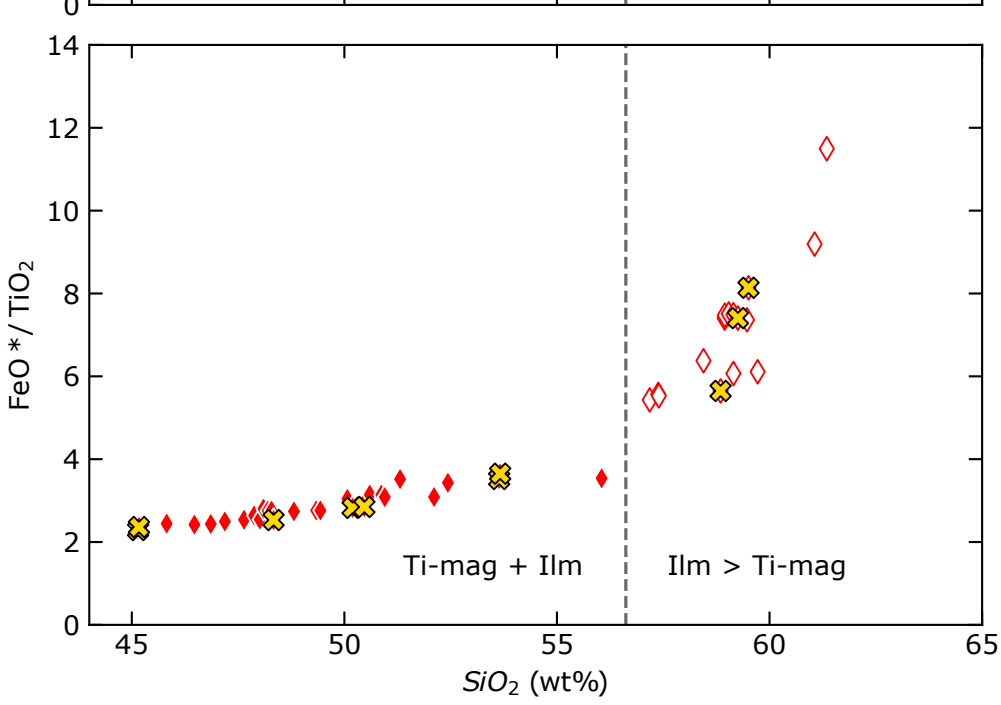
Ti-mag + Ilm
Ilm > Ti-mag
FeO * / TiO2
SiO2 (wt%)

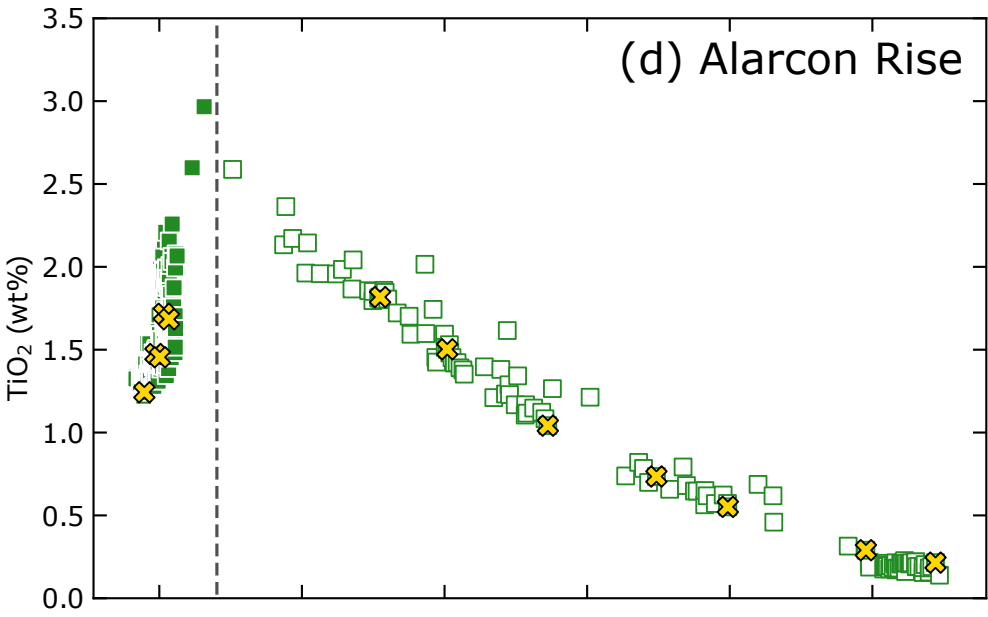
(d) Alarcon Rise
TiO2 (wt%)

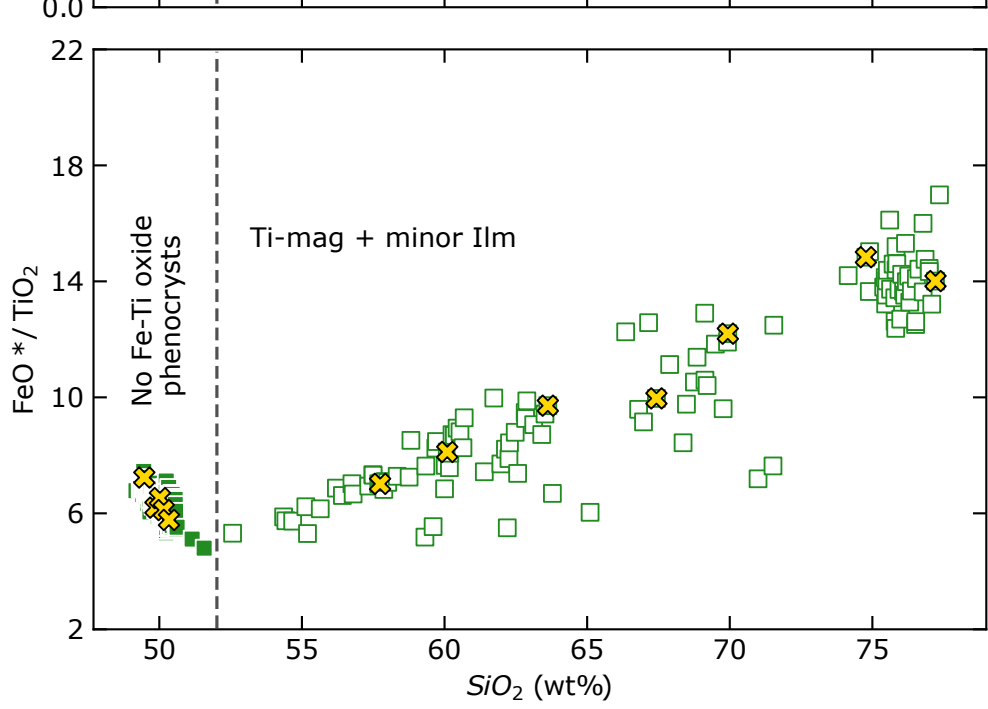
No Fe-Ti oxide phenocrysts
Ti-mag + minor Ilm
FeO * / TiO2
SiO2 (wt%)

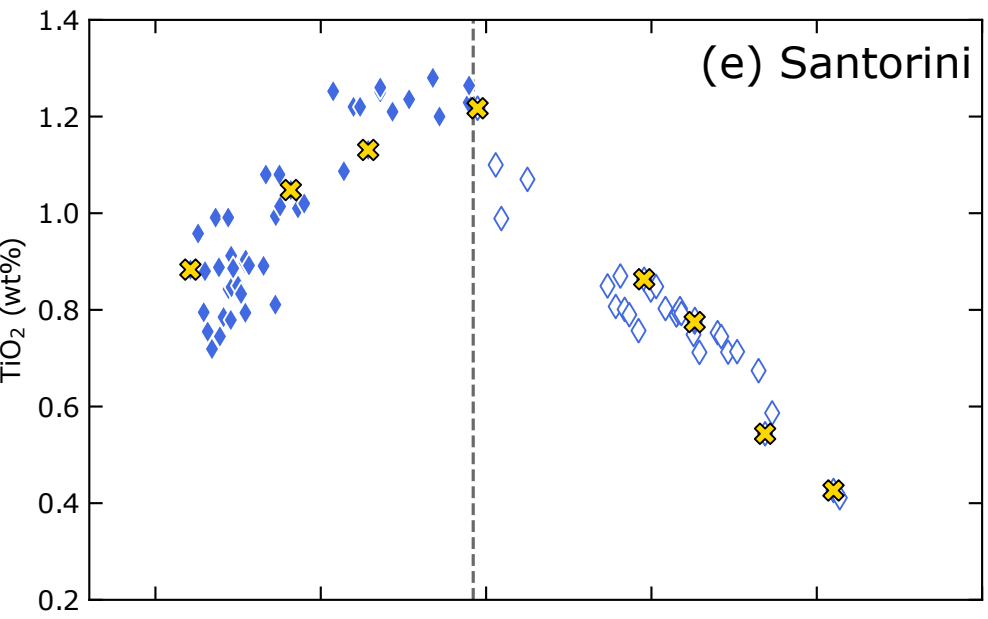
(e) Santorini
TiO2 (wt%)

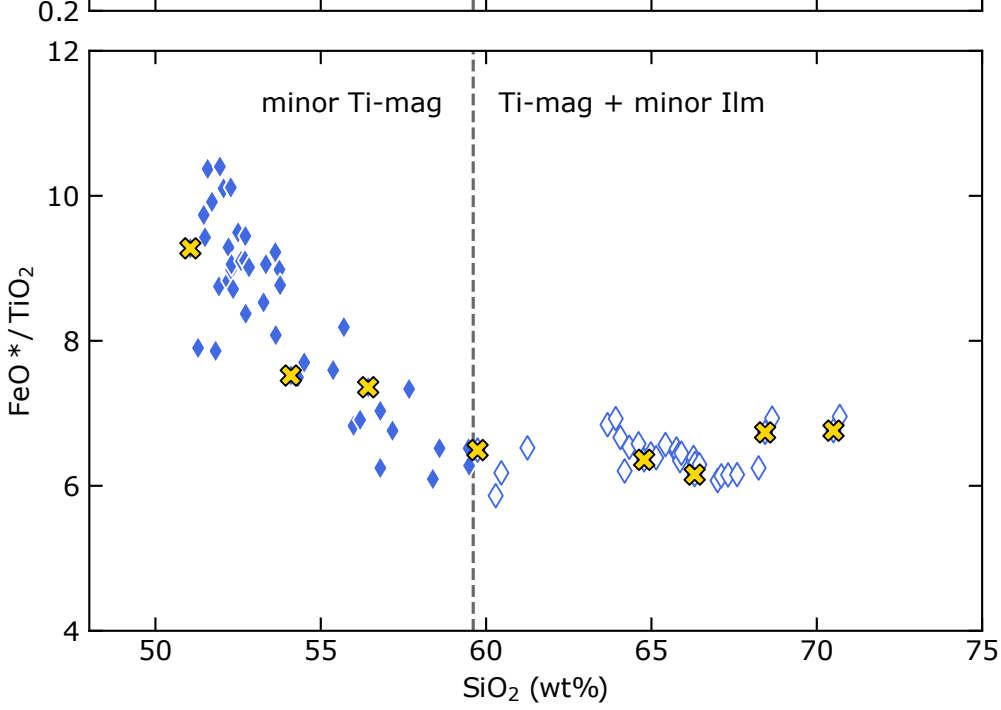
minor Ti-mag
Ti-mag + minor Ilm
FeO * / TiO2
SiO2 (wt%)

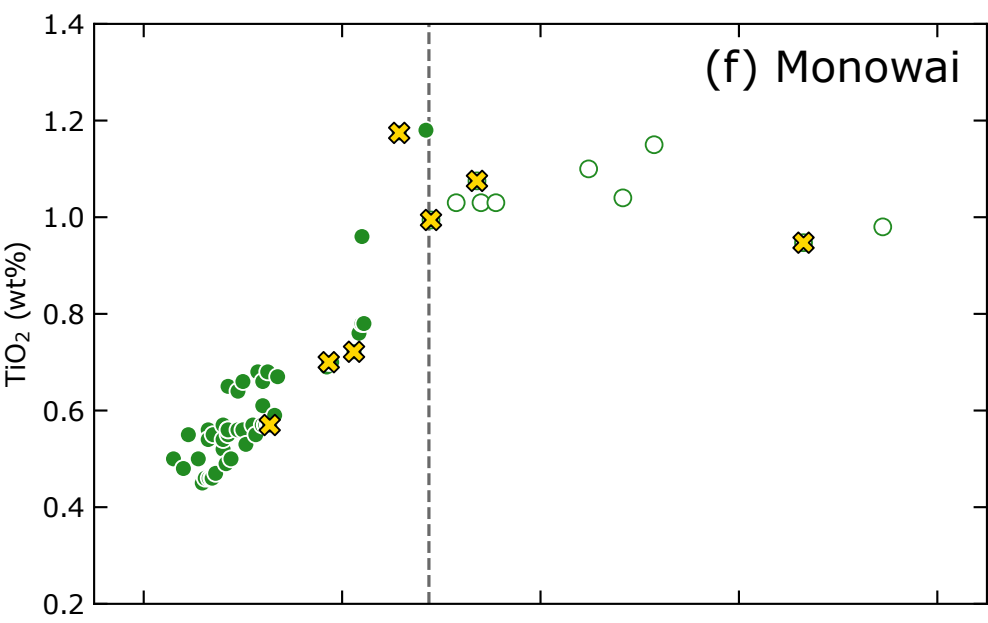
(f) Monowai
TiO2 (wt%)

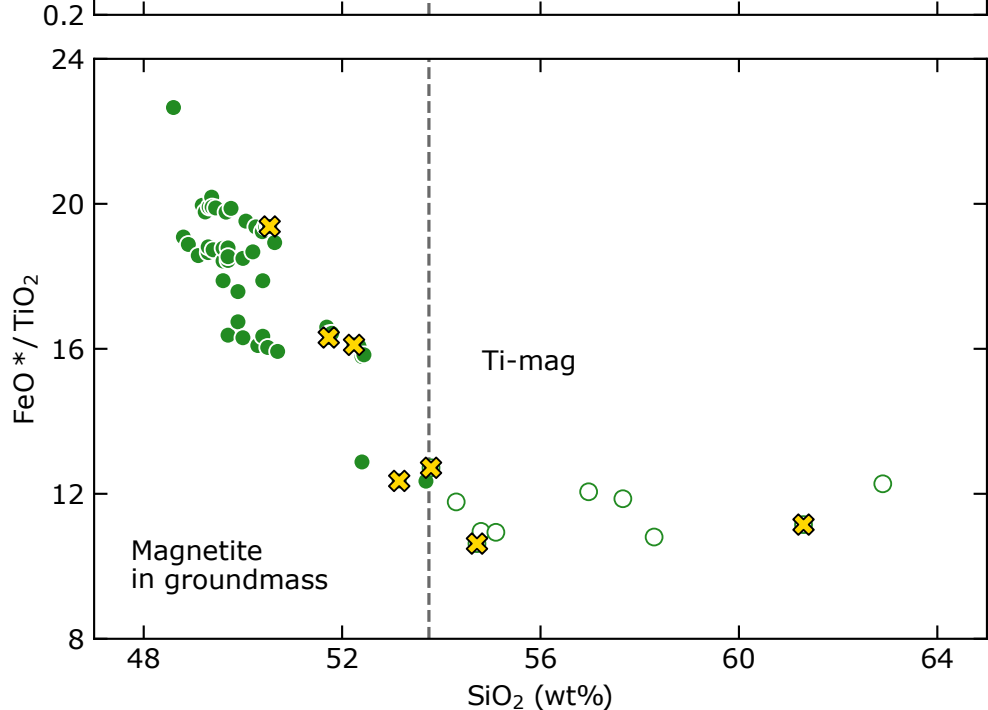
Ti-mag
Magnetite in groundmass
FeO * / TiO2
SiO2 (wt%)

Figure 4

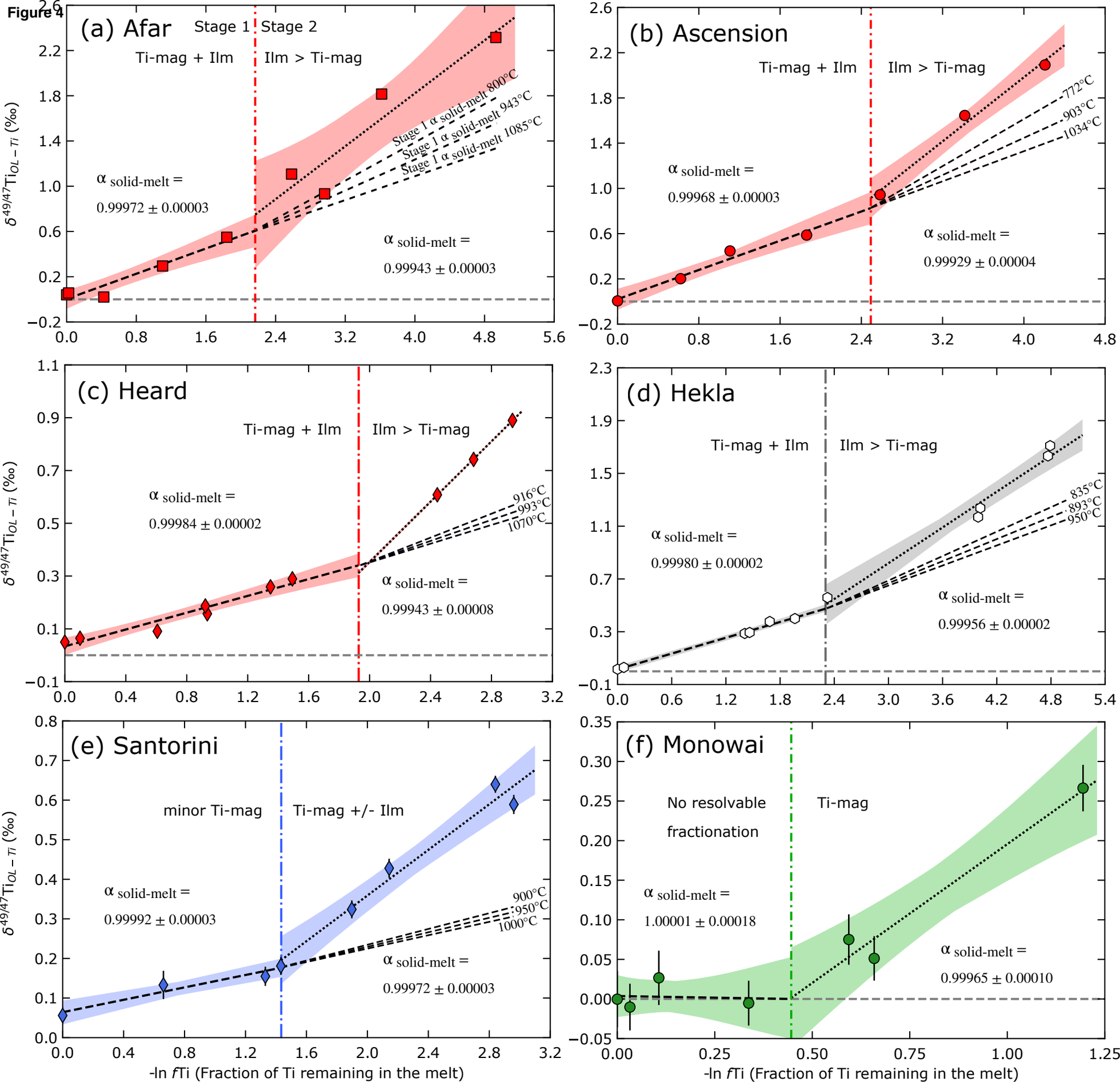
(a) Afar
Stage 1
Stage 2
Ti-mag + Ilm
Ilm > Ti-mag
α solid-melt =
0.99972 ± 0.00003
α solid-melt =
0.99943 ± 0.00003
Stage 1 α solid-melt 800°C
Stage 1 α solid-melt 943°C
Stage 1 α solid-melt 1085°C
(b) Ascension
Ti-mag + Ilm
Ilm > Ti-mag
α solid-melt =
0.99968 ± 0.00003
α solid-melt =
0.99929 ± 0.00004
772°C
903°C
1034°C
(c) Heard
Ti-mag + Ilm
Ilm > Ti-mag
α solid-melt =
0.99984 ± 0.00002
α solid-melt =
0.99943 ± 0.00008
916°C
993°C
1070°C
(d) Hekla
Ti-mag + Ilm
Ilm > Ti-mag
α solid-melt =
0.99980 ± 0.00002
α solid-melt =
0.99956 ± 0.00002
835°C
893°C
950°C
(e) Santorini
minor Ti-mag
Ti-mag +/- Ilm
α solid-melt =
0.99992 ± 0.00003
α solid-melt =
0.99972 ± 0.00003
900°C
950°C
1000°C
(f) Monowai
No resolvable
fractionation
Ti-mag
α solid-melt =
1.00001 ± 0.00018
α solid-melt =
0.99965 ± 0.00010
δ49/47TiOL − Ti (‰)
-ln fTi (Fraction of Ti remaining in the melt)

Figure 5

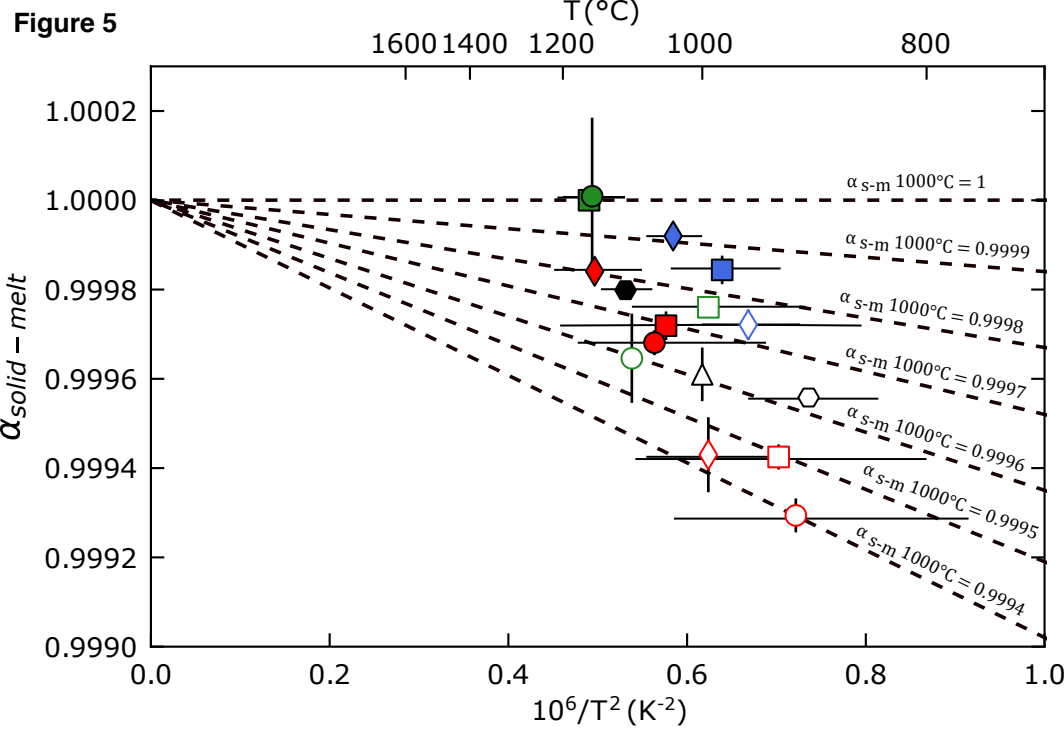

- Afar S1
- Ascension S1
- Heard S1
- Hekla S1 (Deng et al., 2019)
- Kilauea Iki (Johnson et al., 2019)
- Agung (Millet et al., 2016)
- Santorini S1
- Alarcon S1
- Monowai S1
- Afar S2
- Ascension S2
- Heard S2
- Hekla S2 (Deng et al., 2019)
- Santorini S2
- Alarcon S2
- Monowai S2

Figure 6

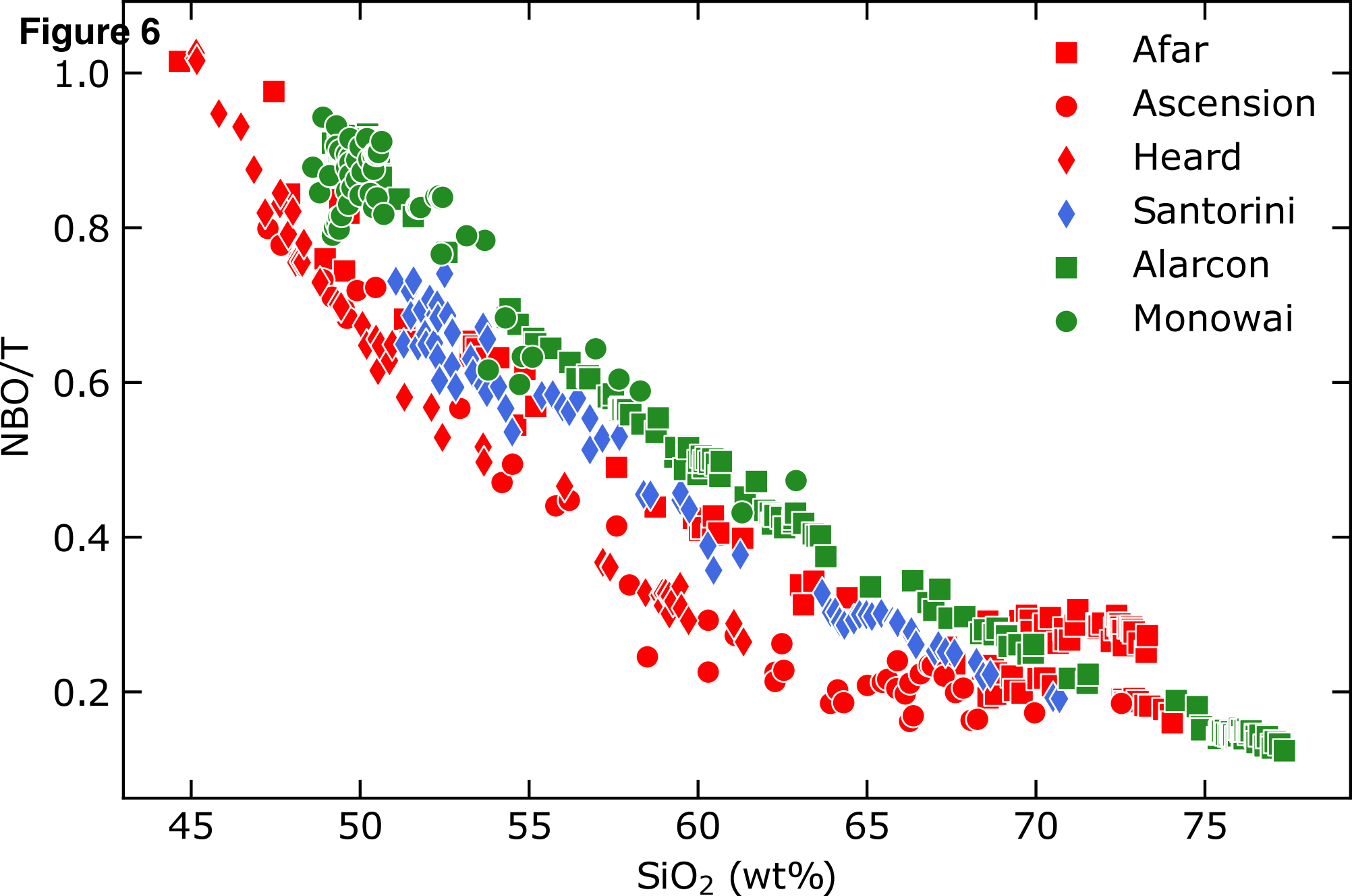
Afar
Ascension
Heard
Santorini
Alarcon
Monowai
NBO/T
1.0
0.8
0.6
0.4
0.2
45
50
55
60
65
70
75
SiO2 (wt%)

Figure 7

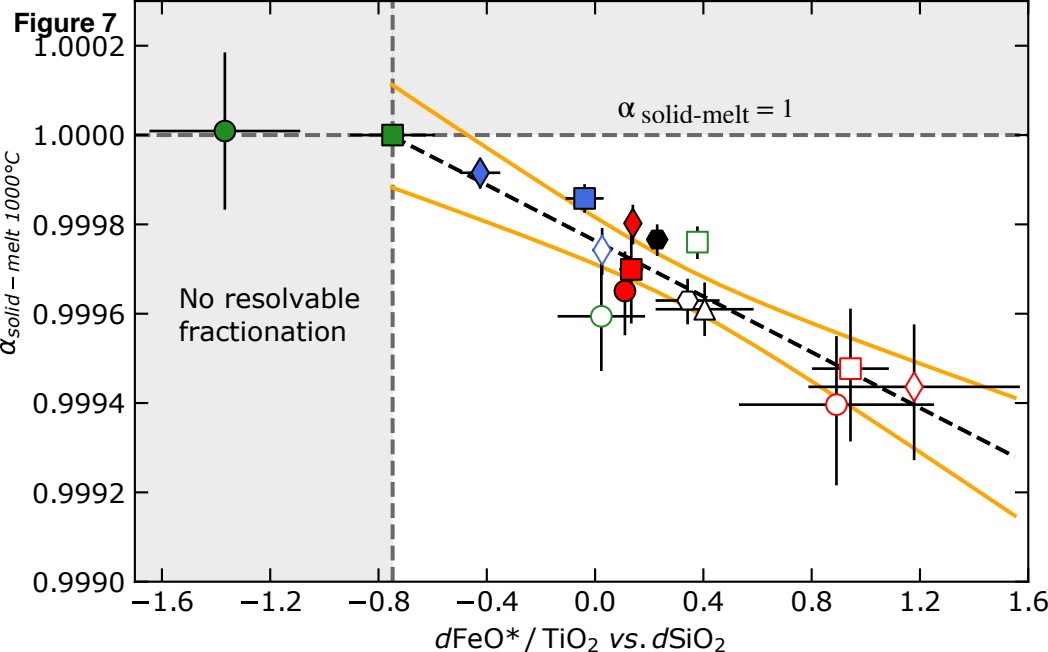
1.0002
1.0000
0.9998
0.9996
0.9994
0.9992
0.9990
$\alpha_{solid-melt\ 1000°C}$
α solid-melt = 1
No resolvable fractionation
−1.6
−1.2
−0.8
−0.4
0.0
0.4
0.8
1.2
1.6
dFeO* / TiO2 vs. dSiO2

Figure 8

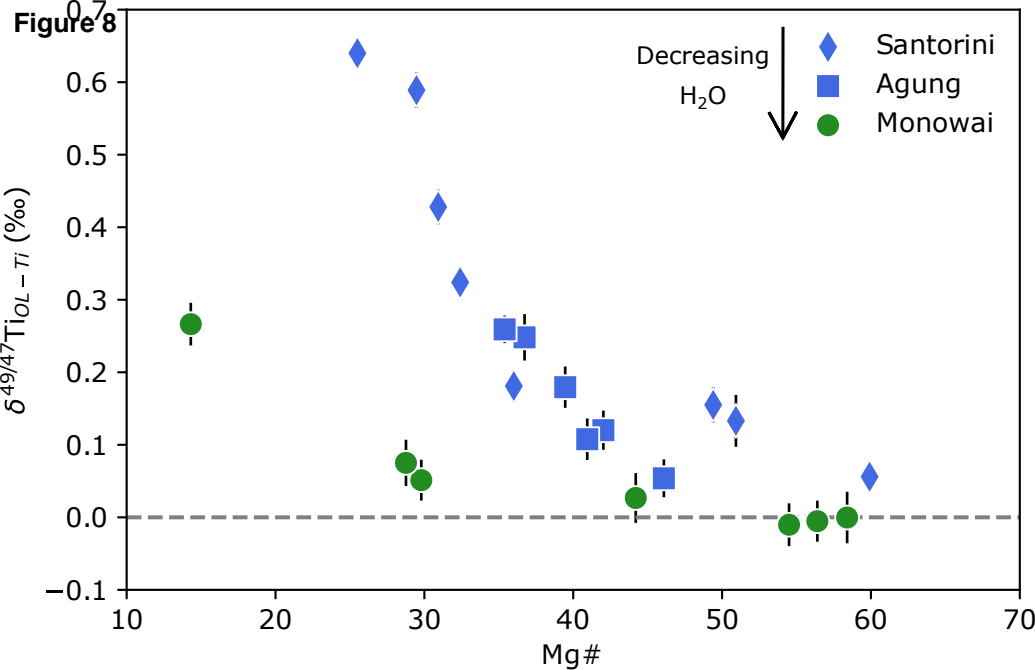
Decreasing
H2O
Santorini
Agung
Monowai
δ49/47TiOL − Ti (‰)
Mg#
0.7
0.6
0.5
0.4
0.3
0.2
0.1
0.0
−0.1
10
20
30
40
50
60
70

Supplementary Figure S1

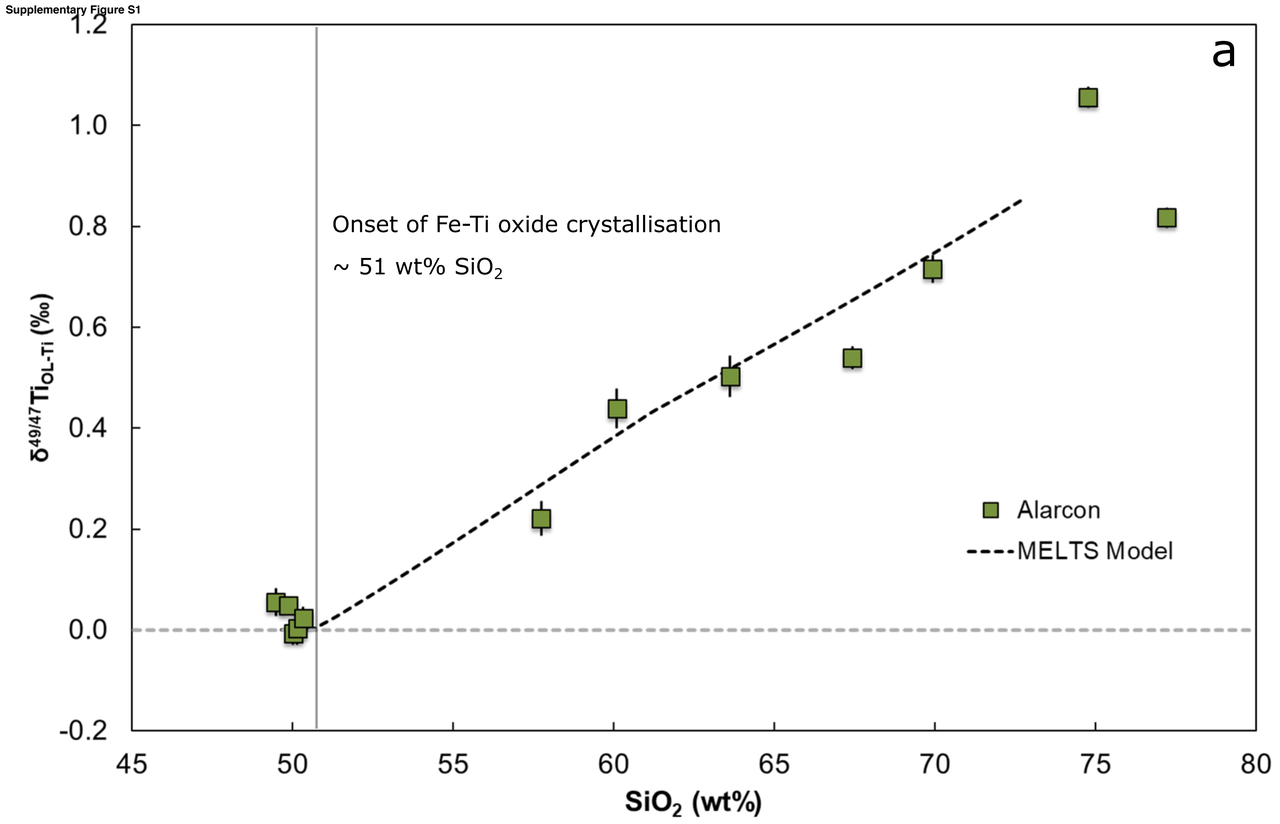

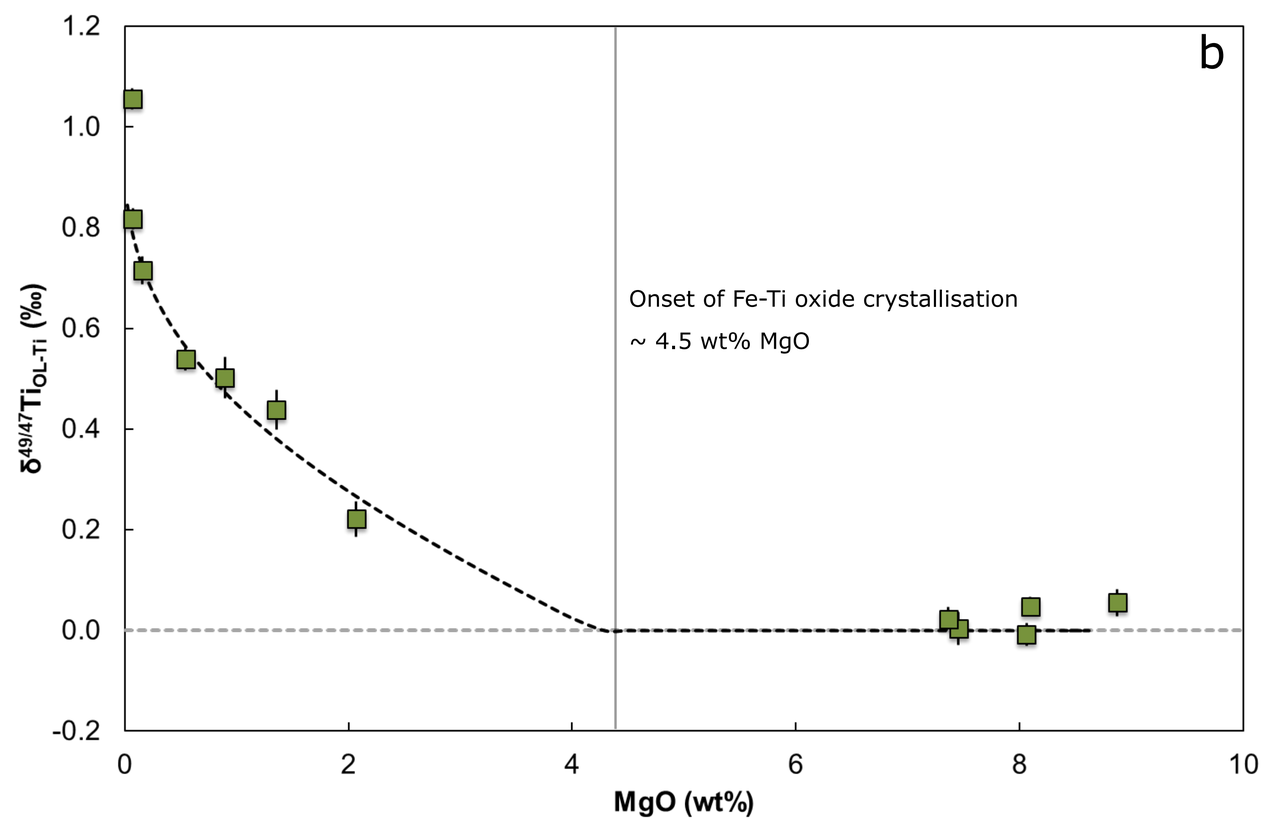

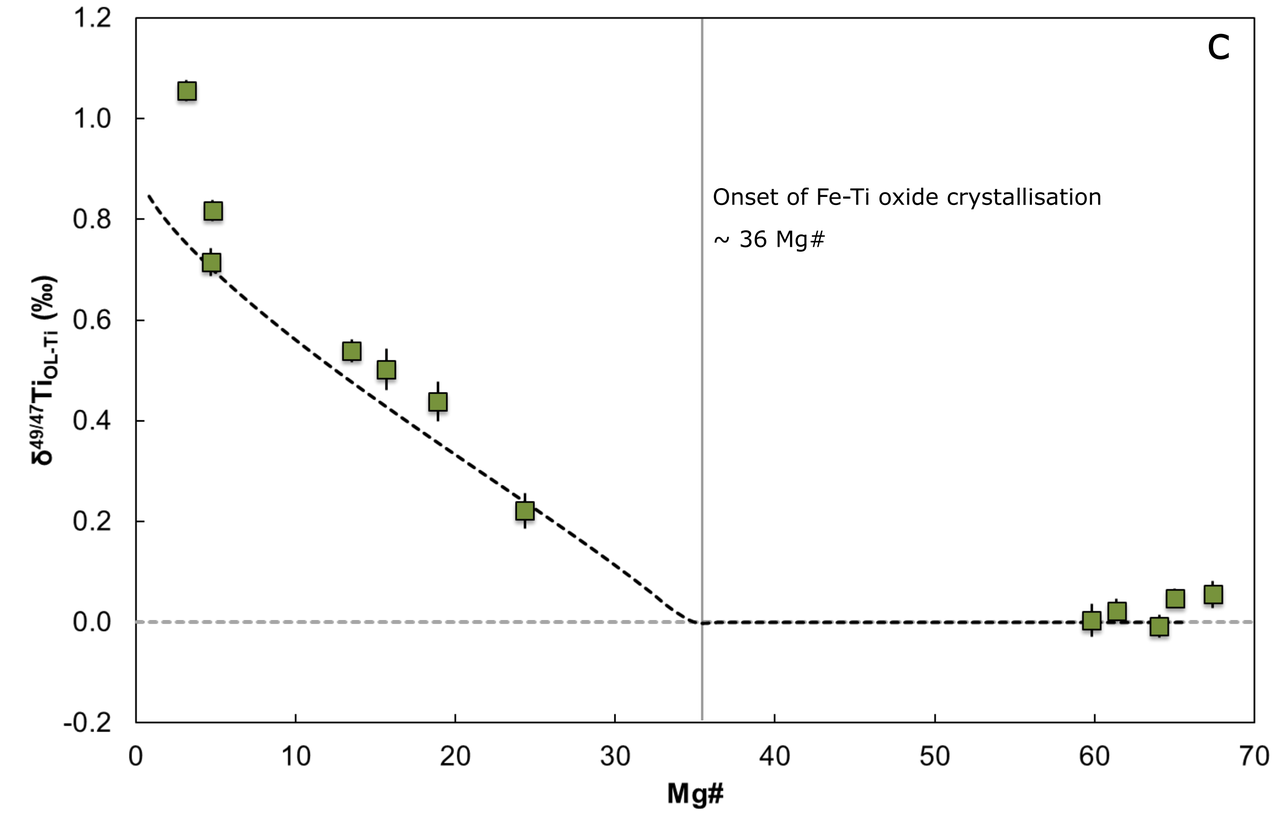

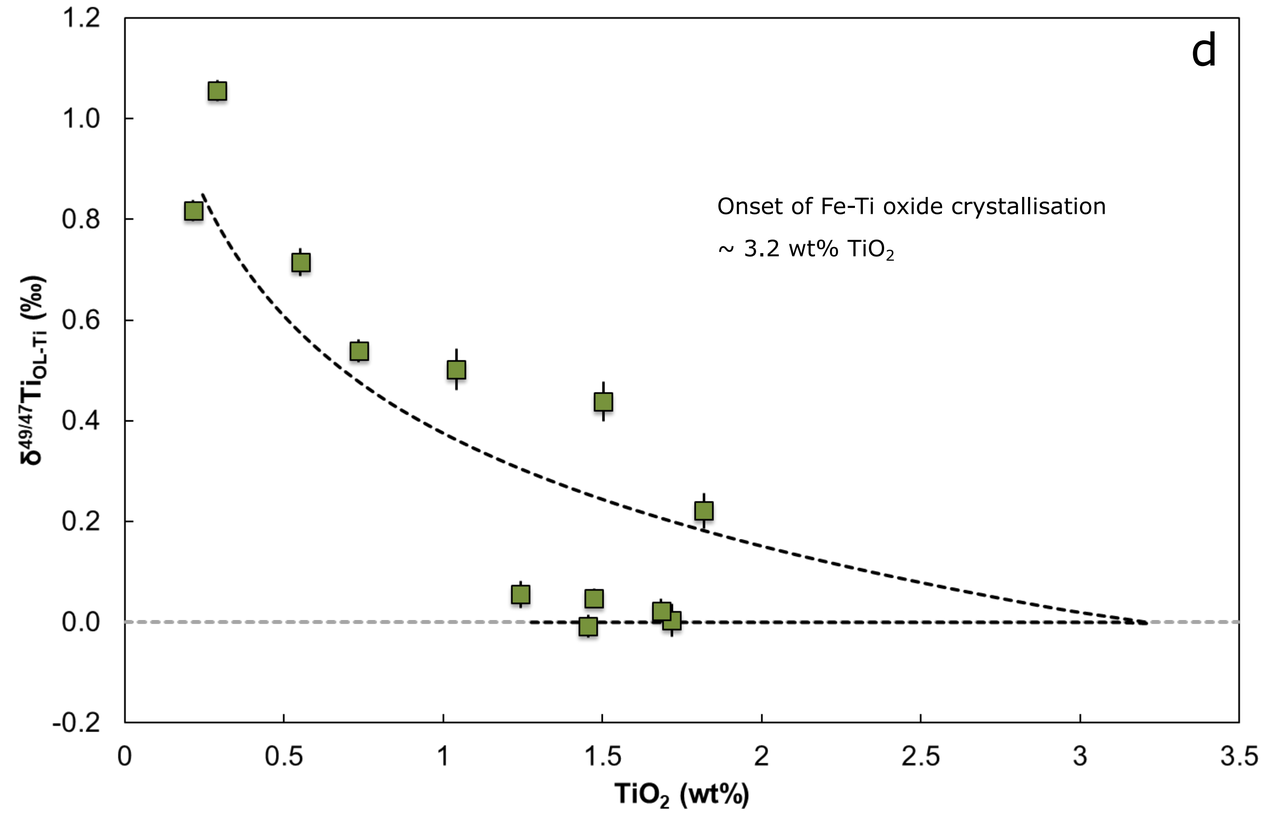

Supplementary Figure S1 - Evolution of Alarcon $\delta^{49/47}$Ti values with respect to a) SiO_2, b) MgO, c) Mg# and, d) TiO_2. The black dashed line represents a fractional crystallisation model produced using Rhyolite-MELTS (Gualda et al., 2012) assigned to fit the Alarcon Rise differentiation suite. Sample D395-R11 was used as a starting composition (see Table S1). Crystallisation occurs conditions similar to those specified in Clague et al. (2018); 0.2 wt% H_2O, an oxidation state of QFM-1 and 800 kbar. Best fit for the data was obtained using a Ti stable isotope fractionation factor between oxides and melt of $\Delta^{49/47}Ti_{oxide\text{-}melt} = -0.38 \times 10^6/T^2$ (with T in K).

Electronic Annex

Click here to download Electronic Annex: Supplementary Table S1 .xlsx

Research Highlights

- Magma series show distinct Ti isotope fractionation patterns during differentiation
- Fe and Ti content of parental melts is the main control on Ti isotope fractionation
- Redox state and water content are secondary controls for arc magmas.

***Declaration of Interest Statement**

Declaration of interests

☒ The authors declare that they have no known competing financial interests or personal relationships that could have appeared to influence the work reported in this paper.

☐The authors declare the following financial interests/personal relationships which may be considered as potential competing interests: